Mathematical modeling of plus-strand RNA virus replication to identify broad-spectrum antiviral treatment strategies

Carolin Zitzmann[1,2,*], Christopher Dächert[3,+], Bianca Schmid[5], Hilde van der Schaar[6,#], Martijn van Hemert[7], Alan S. Perelson[2], Frank J.M. van Kuppeveld[6], Ralf Bartenschlager[4,5,8], Marco Binder[3], Lars Kaderali[1,*]

[1] Institute of Bioinformatics, University Medicine Greifswald, Greifswald, Germany

[2] Theoretical Biology and Biophysics, Los Alamos National Laboratory, Los Alamos, New Mexico, United States of America

[3] Research Group "Dynamics of Early Viral Infection and the Innate Antiviral Response", Division Virus-Associated Carcinogenesis (F170), German Cancer Research Center (DKFZ), Heidelberg, Germany

[4] Division Virus-Associated Carcinogenesis (F170), German Cancer Research Center (DKFZ), Heidelberg, Germany

[5] Dept of Infectious Diseases, Molecular Virology, Heidelberg University, Heidelberg, Germany

[6] Division of infectious Diseases and Immunology, Virology Section, Dept of Biomolecular Health Sciences, Utrecht University, Utrecht, The Netherlands

[7] Department of Medical Microbiology, Leiden University Medical Center, Leiden, The Netherlands

[8] German Center for Infection Research (DZIF), Heidelberg partner site, Heidelberg, Germany

+ Present Address: Max von Pettenkofer Institute, Ludwig-Maximilians-University München, Germany

Present Address: VectorY Therapeutics, Amsterdam, The Netherlands

* Corresponding Authors:

Carolin Zitzmann (czitzmann@lanl.gov), Lars Kaderali (lars.kaderali@uni-greifswald.de)

Funding information

This work received funding from the BMBF through the ERASysAPP project SysVirDrug (grant 031A602A). LK received funding from the DFG (grant number KA 2989/13-1). C.D. was supported by a stipend of the DKFZ International PhD Program. Portions of this work were done under the auspices of the U.S. Department of Energy under contract 89233218CNA000001 and supported by NIH grants R01-

OD011095, R01-AI078881, and R01-AI116868 to ASP. The funders had no role in study design, data collection and analysis, decision to publish, or preparation of the manuscript.

Abstract

Plus-strand RNA viruses are the largest group of viruses. Many are human pathogens that inflict a socio-economic burden. Interestingly, plus-strand RNA viruses share remarkable similarities in their replication. A hallmark of plus-strand RNA viruses is the remodeling of intracellular membranes to establish replication organelles (so-called “replication factories”), which provide a protected environment for the replicase complex, consisting of the viral genome and proteins necessary for viral RNA synthesis. In the current study, we investigate pan-viral similarities and virus-specific differences in the life cycle of this highly relevant group of viruses. We first measured the kinetics of viral RNA, viral protein, and infectious virus particle production of hepatitis C virus (HCV), dengue virus (DENV), and coxsackievirus B3 (CVB3) in the immuno-compromised Huh7 cell line and thus without perturbations by an intrinsic immune response. Based on these measurements, we developed a detailed mathematical model of the replication of HCV, DENV, and CVB3 and show that only small virus-specific changes in the model were necessary to describe the *in vitro* dynamics of the different viruses. Our model correctly predicted virus-specific mechanisms such as host cell translation shut off and different kinetics of replication organelles. Further, our model suggests that the ability to suppress or shut down host cell mRNA translation may be a key factor for *in vitro* replication efficiency which may determine acute self-limited or chronic infection. We further analyzed potential broad-spectrum antiviral treatment options *in silico* and found that targeting viral RNA translation, especially polyprotein cleavage, and viral RNA synthesis may be the most promising drug targets for all plus-strand RNA viruses. Moreover, we found that targeting only the formation of replicase complexes did not stop the viral replication *in vitro* early in infection, while inhibiting intracellular trafficking processes may even lead to amplified viral growth.

Author summary

Plus-strand RNA viruses comprise a large group of related and medically relevant viruses. The current global pandemic of COVID-19 caused by the SARS-coronavirus-2 as well as the constant spread of diseases such as dengue and chikungunya fever show the necessity of a comprehensive and precise analysis of plus-strand RNA virus infections. Plus-strand RNA viruses share similarities in their life cycle. To understand their within-host replication strategies, we developed a mathematical model that studies

pan-viral similarities and virus-specific differences of three plus-strand RNA viruses, namely hepatitis C, dengue, and coxsackievirus. By fitting our model to *in vitro* data, we found that only small virus-specific variations in the model were required to describe the dynamics of all three viruses. Furthermore, our model predicted that ribosomes involved in viral RNA translation seem to be a key player in plus-strand RNA replication efficiency, which may determine acute or chronic infection outcome. Furthermore, our *in-silico* drug treatment analysis suggests that targeting viral proteases involved in polyprotein cleavage, in combination with viral RNA replication, may represent promising drug targets with broad-spectrum antiviral activity.

Introduction

Plus-strand RNA viruses are the largest group of human pathogens that cause re-emerging epidemics as seen with dengue, chikungunya and Zika virus, as well as global pandemics of acute and chronic infectious diseases such as hepatitis C and the common cold. The current global SARS-coronavirus-2 (SARS-CoV-2) pandemic shows how our lives can become affected by a rapidly spreading plus-strand RNA virus. As of May 2022, more than 500 million cases of SARS-CoV-2 infections have been reported with over 6 million confirmed deaths [1,2]. While a global pandemic of the current scale clearly causes an exceptional socio-economic burden [3], various other plus-strand RNA viruses cause significant burden as well. For example, in 2013, symptomatic dengue cases in 141 countries caused socio-economic costs of US$ 8.9 billion [4], while the costs of the latest Zika outbreak has been estimated as US$ 7-18 billion in Latin America and the Caribbean from 2015 to 2017 [5]. Furthermore, between 2014 and 2018, the USA spend around US$ 60 billion for hepatitis C medication with around US$ 80,000 per patient [6,7].

Treatment options are limited for the majority of plus-strand RNA viruses. While there are vaccines and vaccine candidates available for few viruses, approved direct acting antivirals are only available against hepatitis C and SARS-CoV-2 [8,9]. Given the high disease burden and socio-economic cost caused by infections with plus-strand RNA viruses, there is an urgent need for broadly acting antiviral drugs. To develop these, it is important to study the life cycles and host restriction and dependency factors in detail, not only at the level of each virus individually, but also across a group of related viruses to gain pan-viral insights. In the current study, we investigated the life cycle of plus-strand RNA viruses. The ultimate goal was to reveal commonly effective antiviral strategies and potential therapeutic target

processes in the viral life cycle. To do so, we chose three representatives of plus-strand RNA viruses, hepatitis C, dengue, and coxsackievirus B3 (compare Table 1).

The enveloped blood-borne hepatitis C virus (HCV) is a *Hepacivirus* of the family *Flaviviridae* that causes acute and chronic hepatitis C. An acute infection is typically mild, but once chronic and untreated, may cause life threatening conditions, including liver cirrhosis and hepatocellular carcinoma. Approximately 70 million people worldwide live with chronic hepatitis C, with 400,000 related deaths annually [10]. Notably, hepatitis C can be cured in more than 95% of cases with direct acting antivirals that inhibit viral replication [10].

The re-emerging dengue virus (DENV) is a *Flavivirus* and belongs, as HCV, to the family *Flaviviridae*. Annually, DENV infects 390 million people worldwide, with around 96 million of them becoming symptomatic. Unlike HCV, DENV is vector-borne and is spread mainly by the mosquitoes of the *Aedes* species. Infection with DENV causes flu-like illness, occasionally with severe complications mostly associated with heterotypic secondary infections (e.g. hemorrhagic fever and shock syndrome) [11]. The clinical manifestation of a DENV infection is closely related to infections with the mosquito-borne chikungunya and Zika virus, leading to frequent misdiagnosis [12].

Coxsackieviruses are members of the genus *Enterovirus* of the family *Picornaviridae*. This genus includes important human pathogens such as poliovirus, enterovirus-A71 (EV-A71), EV-D68, coxsackievirus, and rhinovirus. Enteroviruses cause 10 to 15 million infections every year and therefore belong to the most prevalent pathogens [13]. Enteroviruses cause a variety of diseases, including hand-foot-and-mouth disease, encephalitis, meningitis, and paralysis [14]. Coxsackie B viruses are also known to infect cardiac tissue, leading to viral myocarditis, which can develop to congestive heart failure [15]. In this study, we focus on coxsackievirus B3 (CVB3).

Despite their broad range of clinical manifestations, transmission routes, and tropism (Table 1), plus-strand RNA viruses share remarkable similarities in their replication strategy. By definition, the genome of plus-strand RNA viruses has the polarity of cellular mRNAs. Therefore, after delivery into cells, the genome is directly translated, giving rise to a polyprotein that must subsequently be cleaved into viral proteins. These proteins induce host cell membrane rearrangements forming replication organelles (ROs). Either within those ROs or on its outer membrane facing the cytosol, viral RNAs are amplified by

124 the viral replicase complex comprising, amongst others, the RNA-dependent RNA polymerase (RdRp).
125 These ROs are thought to serve hiding viral RNAs from host immune response and thus to protect them
126 from degradation. In addition, the membranous compartment allows the coordinated coupling of
127 different steps of the viral replication cycle, i.e., RNA translation, RNA replication, and virion assembly
128 [16–19].
129
130 However, there are striking differences in the viral life cycles of the three studied viruses. For example,
131 the morphology of ROs in which replication takes place differs considerably. While HCV forms double
132 membrane vesicles (DMV), DENV induces invaginations of host cellular membranes [20]. CVB3 infection
133 first results in single-membrane tubular structures that subsequently transform into DMVs and
134 multilamellar vesicles [21]. Additionally, HCV and DENV as representatives of *Flaviviridae* remodel
135 membranes of the rough endoplasmic reticulum (rER), however, the *Picornaviridae* CVB3 uses the ER
136 and Golgi apparatus for its RO formation [20]. Another interesting feature of CVB3 is its ability to trigger
137 a so-called host translational shut-off, leading to increased viral over host RNA translation[22].
138 Repressed host RNA translation has also been reported for DENV [23], however, a host shut-off has not
139 been reported for HCV, which instead shows parallel translation of viral and host cell RNAs, consistent
140 with the predominantly chronic infection caused by this virus [24].
141
142 To identify an efficient, broadly active treatment strategy against viral infectious diseases, a
143 comprehensive knowledge of viruses as well as their exploitive interaction with the host is of major
144 importance. Mathematical modeling has proven to be a powerful tool to study viral pathogenesis,
145 transmission, and disease progression and has increased our knowledge about therapeutic intervention
146 and vaccination as well as the involvement of the immune system for viruses such as the human
147 immunodeficiency virus (HIV), HCV, influenza A virus, DENV, Zika virus, and SARS-CoV-2 [25–31]. One of
148 the major strengths of mathematical models is their ability to describe and analyze viral replication in a
149 quantitative, dynamic (time-resolved) framework, and to characterize the influence individual
150 parameters have on the ensuing dynamics. These models thus permit much deeper insights into viral
151 replication and antiviral strategies than static, often more qualitative snapshots of host-pathogen
152 interactions.
153
154 In the current study, we reproduced the dynamics of the initial post infection phase of the life cycle of
155 three representative plus-strand RNA viruses, namely HCV, DENV, and CVB3, with one common

mathematical model. Using the model, we identified pan-viral similarities and virus-specific differences in the life cycle of plus-strand RNA viruses that are represented by a unique set of model parameters. The inter-viral differences among the plus-strand RNA viruses under investigation have been further analyzed to study how these differences might be related to clinical disease manifestation, particularly with regard to chronic versus acute infections. Our model suggests that the number of ribosomes available for viral RNA translation may be a crucial factor for either acute or chronic infection outcome. Furthermore, we studied broad-spectrum antiviral treatment options and found inhibiting viral proteases involved in polyprotein cleavage, and RNA synthesis are promising drug targets.

Table 1: *Feature comparison of plus-strand RNA viruses. DMV: double membrane vesicles, ER: endoplasmic reticulum, NS: non-structural, S: structural*

	HCV	**DENV**	**CVB3**
Virus characteristics			
Family	Flaviviridae [20]	Flaviviridae [20]	Picornaviridae [20]
Genus	Hepacivirus [20]	Flavivirus [20]	Enterovirus [20]
Transmission	Human-to-human [20]	Mosquito-to-human [32]	Human-to-human [15]
Tropism	Hepatocytes [33]	Dendritic cells, monocytes, macrophages [32]	Brain/neuron, cardiac tissue, hepatocytes [15,34,35]
Genome size	9.6 kb [33]	10.7 kb [32]	7.5 kb [15]
Number of genes/encoded proteins	10 (3 S and 7 NS proteins) [33]	10 (3 S and 7 NS proteins) [32]	11 (4 S and 7 NS proteins) [15]
Replication organelle (RO)	DMV derived from ER [20]	Invaginated vesicles derived from ER [20]	DMV derived from Golgi and ER [20]
Enveloped	Yes [20]	Yes [20]	No [20]
Host shut-off of RNA translation	No [24]	Partially [23]	Yes [22]
Disease characteristics			
Infection outcome	Acute and chronic [36]	Acute [37]	Primary acute (ability of virus persistence) [15,38]

Basic reproductive number (R_0)	1-3 (strain dependent)[39]	5 [40]	2.5 to 5.5 (range for different enteroviruses [41,42])
Incubation period	2 weeks to 6 months [36]	4 to 10 days [37]	5 days [38]
Exponential growth rate	Measured in human blood: 2.2 per day (doubling time 7.6 hours) [43]	Primary infection measured in human blood: 4.0 per day (doubling time 4.2 hours) [approximated from [44]]	Measured in mouse blood: 4.5 per day (doubling time 3.7 hours) [approximated from [38]]
	Measured in chimpanzees: 1st phase: 1.4 per day (doubling time 12 hours) [45] 2nd phase: 0.1 per day (doubling time 7.5 days) [45]	Secondary infection measured in human blood: 4.6 per day (doubling time 3.6 hours) [approximated from [44]]	Measured in mouse heart: 14.5 per day (doubling time 1.1 hours) [approximated from [38]]
Time to reach peak	Measured in human blood: 21 days [43]	Measured in human blood: 7 days [44]	Measured in mouse blood and heart: 3 days [38]
Peak viral load	Measured in human and chimpanzee blood: 10^6 to 10^7 RNA per ml [43,45,46] Measured in human liver: 10^8 RNA per g [43]	Measured in human blood: 10^9 to 10^{10} RNA per ml [44]	In mouse blood: 10^6 RNA per ml [38] In mouse heart: 10^{11} to 10^{12} RNA per g [38]
RNA clearance	Individuals with spontaneous clearance: 4.3 per day (RNA half-life 4 hours) [approximated from [47]]	Primary infection measured in human blood: 2.8 per day (RNA half- life 6 hours) [approximated from [44]]	Measured in mouse blood: 0.7 per day (RNA half- life 24 hours) [approximated from [38]]
	otherwise: persistent RNA [47]	Secondary infection measured in human blood: 4.0 per day (RNA half- life 4.2 hours) [approximated from [44]]	Measured in mouse heart: 1st phase: 1.2 per day (RNA half- life 13.4 hours) [approximated from [38]] 2nd phase: 0.05 per day (RNA half- life 14

			days) [approximated from [38]]
Infection duration	Months to Years [36]	2 to 3 weeks [44]	2 weeks [48]

Methods

Kinetic experiments and infectivity titers

HCV infections: 2x10^5 Lunet-$CD81_{high}$ [49] cells per 6-well were seeded in 2 mL 16 hours prior to infection. To ensure simultaneous infection of all cells, cells were kept at 4°C for 30 min before medium aspiration and inoculation with pre-cooled PEG-precipitated HCV_{cc} (Jc1) [50] at an MOI of 1 at 4°C for one hour (1 mL per 6-well). The inoculum was removed and cells were covered with 1 ml per well pre-warmed (37°C) medium and incubated for one hour at 37°C. Medium was aspirated and cells were treated with an acid wash protocol to remove extracellular vesicles and unbound virus particles: cells were washed with an acidic solution (0.14 M NaCl, 50 mM Glycine/HCl, pH 3.0, 670 µL per 6-well) for three minutes at 37°C before neutralization with neutralization buffer (0.14 M NaCl, 0.5 M HEPES, pH 7.5, 320 µL per 6-well) and one wash with pre-warmed medium. After that, fresh medium was added. After indicated time-points, total cellular RNA was extracted by phenol-chloroform extraction. Infected cells were washed prior to lysis according to the acid wash protocol described above. After three washing steps with cold 1x PBS, cells were lysed in GITC buffer (700 µL per 6 well) and RNA was extracted as described [51]. A strand-specific RT-qPCR protocol was used to quantify numbers of (+)- and (-)-strand RNA per cell [52]. TCID50 of supernatants was measured and calculated as described previously [50] and converted to PFU/mL.

CVB3 infections: CVB3 wild-type (wt) and CVB3-Rluc, which carries *Renilla luciferase* upstream of the P1 region, were generated as described previously [53]. Subconfluent monolayers of HuH7 cells, provided by prof. R. Bartenschlager, were infected with CVB3 wt or CVB3-Rluc at an MOI of 1 for 45 minutes. After removal of the viral inoculum, cells were washed once with PBS and fresh medium (DMEM supplemented with 10% FBS and penicillin and streptomycin) was added. Every hour up to 9 hours post-infection, cells were collected and subjected to various assays. Each assay was performed on three biological replicates. Cells were either frozen together with the medium, after which progeny virus titers were determined by endpoint titration by the method of Reed and Muench and converted to PFU/mL.

Another set of cells were lysed in buffer to determine the luciferase activity as a measure of viral protein translation as described previously [53]. Lastly, cells frozen after aspiration of the medium were used for total RNA isolation and quantification of the amount of viral RNA copies per cell with quantitative PCR as described previously [54].

DENV infections: DENV kinetic measurements of intracellular plus-strand RNA and luciferase activity as well as extracellular infectious virus titers have been taken from [55]. In brief, $2x10^5$ Huh7 cells were infected with DENV reporter virus expressing Renilla luciferase [56] at an MOI of 10. RNA extraction and qRT-PCR as well as Renilla luciferase activity were analyzed from cell lysates. RNA was normalized to the 2 h value. Infectivity titers (TCID50/mL) were measured from viral supernatant by limited dilution assays and converted to PFU/mL, supernatants were subsequently supplemented [55].

Plus-strand RNA virus replication model

We developed a mechanistic model using ordinary differential equations (ODEs) and mass action kinetics to analyze pan-viral similarities and virus-specific differences within the plus-strand RNA virus life cycle. Our published models on two plus-strand RNA viruses, HCV and DENV, served as a basis for the pan-viral plus-strand RNA virus replication model [19,55,57]. However, in our previous published models, we studied host dependency factors responsible for cell line permissiveness and restriction factors such as the innate immune response. Therefore, those models were modified to reflect merely the plus-strand RNA life cycle from virus entry to release of all viruses considered here.

The resulting model of plus-strand RNA virus replication is composed of four main processes: Entry of plus-strand RNA virus via receptor-mediated endocytosis and release of the viral genome (Fig 1 steps ① and ②), its subsequent translation into viral proteins (Fig 1 steps ③ to ⑤), viral RNA replication within the replication organelle (Fig 1 steps ⑥ to ⑨), and further replication (Fig 1 step ⑩) or RNA export out of the replication organelle (Fig 1 step ⑪) or virus packaging and release from the cell with subsequent re-infection of the same cell or infection of naïve cells (Fig 1 steps ⑫ and ⑬).

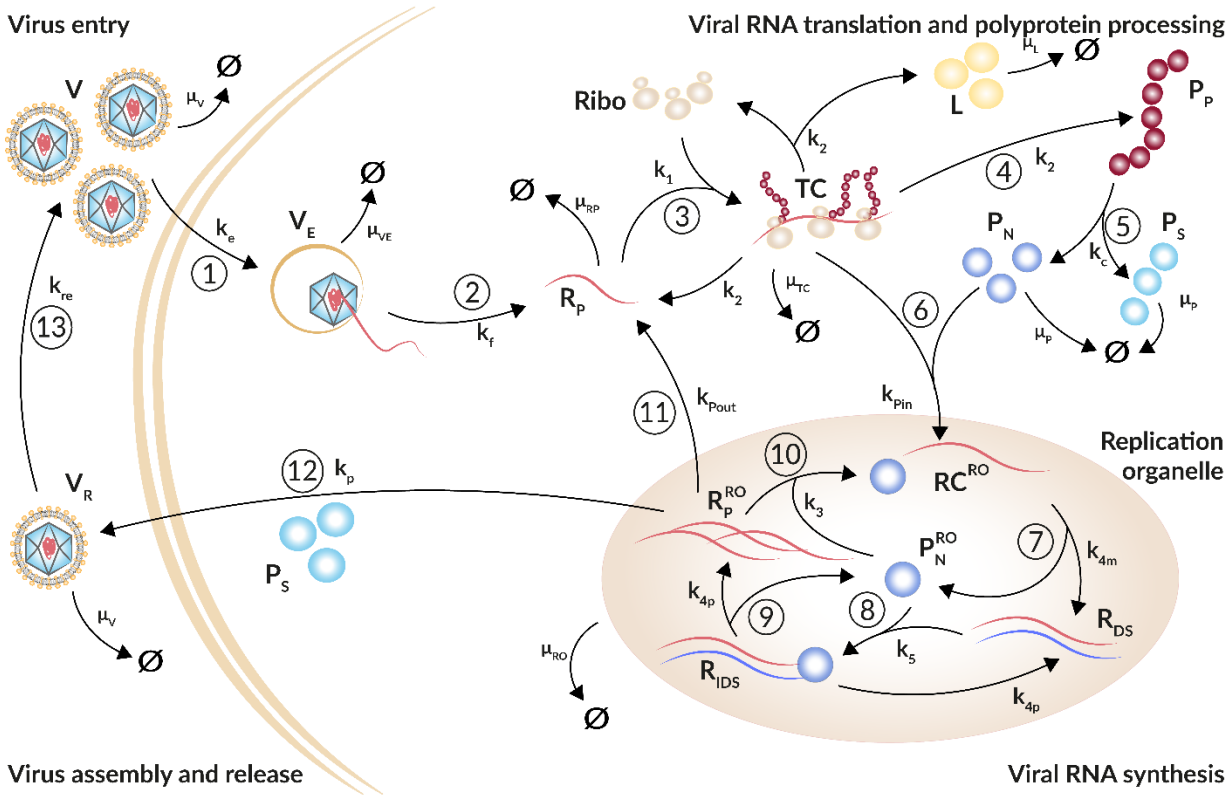

Figure 1: Schematic illustration of the plus-strand RNA life cycle. ① *Virus* (V) *enters the cell via receptor-mediated endocytosis* (k_e). ② *The viral genome* (R_P) *is released* (k_f). *Virus within the endosome* (V_E) *degrades with rate constant* μ_{VE}. ③ *Ribosomes* $(Ribo)$ *bind the viral genome and form (* k_1*) a translation initiation complex* (TC) *that degrades with rate constant* μ_{TC}. ④ *The viral genome* (R_P) *is translated* (k_2) *into a polyprotein* (P_P) *that* ⑤ *is subsequently cleaved* (k_c) *into structural and non-structural viral proteins,* P_S *and* P_N*, respectively. To measure translation activity, luciferase (L) is integrated into the viral genome and produced with RNA translation. Viral proteins degrade with rate constant* μ_P*; luciferase degrades with rate constant* μ_L. ⑥ *Non-structural proteins and freshly translated viral RNA form* (k_{Pin}) *replicase complexes* (RC) *that are associated with replication organelles (ROs) and* ⑦ *serve as a template for the minus-strand synthesis* (k_{4m}) *leading to double-stranded RNA* (R_{DS}).⑧ *Viral non-structural proteins, such as the RdRp, within the replication organelle* (P_N^{RO}) *bind to double-stranded RNA forming* (k_5) *a minus-strand replication intermediate complex* (R_{IDS}) *that* ⑨ *initiates plus-strand RNA synthesis* (k_{4p}) *giving rise to multiple copies of viral plus-strand RNA* (R_P^{RO}). *All species within the replication organelle degrade with the same rate constant* μ_{RO}. ⑩ *The viral genome can remain within the replication organelle, where it undergoes multiple rounds of genome replication* (k_3), ⑪ *it*

can be exported (k_{Pout}) out of the replication organelle into the cytoplasm starting with the translation cycle again, or ⑫ the plus-strand RNA genome (R_P^{RO}) is packaged together with structural proteins (P_S) into virions (V_R) that are released from the cell (k_p) and ⑬ may re-infect the same cell or infect naïve cells (k_{re}). Extracellular infectious viral species (V and V_R) degrade with rate constant μ_V.

The virus infection process (Eqs. 1 and 2), i.e., receptor-mediated virus entry, fusion, and release of the viral genome into the cytoplasm, as well as re-infection of the same cell or further infection of naïve cells (Eq. 14) are represented by extracellular virus V, virus within endosomes V_E, and newly produced virus released from infected cells V_R and are given by the equations

$$\frac{dV}{dt} = -k_e^i V + k_{re} V_R - \mu_V^i V \#(1)$$

and

$$\frac{dV_E}{dt} = k_e^i V - k_f^i V_E - \mu_{V_E} V_E . \#(2)$$

Extracellular virus V enters a single cell via receptor-mediated endocytosis with rate constant k_e^i or degrades with constant rate μ_V^i. Note that virus-specific parameters are marked with a superscripted i with $i \in \{HCV, DENV, CVB3\}$. Virus within endosomes V_E either degrades with rate constant μ_{VE} or undergoes conformational changes of its nucleocapsid resulting in the release of the viral genome R_P with rate constant k_f^i. Note that extracellular virus is also replenished by the release of virus from the cell at rate k_{re}.

Viral RNA translation and replication (Eqs. 3 to 13) are modeled based on our published HCV and DENV models [19,55]. In brief, our model describes the translation associated processes in the cytoplasm (Eqs. 3 to 8) starting with free viral RNA R_P in the cytoplasm, an intermediate translation initiation complex TC, as well as the translated polyprotein P_P which is cleaved into structural and non-structural viral proteins, P_S and P_N, respectively. Note that a firefly luciferase gene has been integrated into the viral genomes. The luciferase activity L was measured from cell lysates as a marker for translation activity (see Methods) reflecting protein concentration and has been introduced into the model. Translation and polyprotein processing are modeled with the following ODEs, where $Ribo_{tot}^i$ and RC_{MAX} are the total number of ribosomes and maximal number of replicase complexes in a cell (see below for details), respectively:

$$\frac{dR_P}{dt} = k_f^i V_E - k_1 R_P\left(Ribo_{tot}^i - TC\right) + k_2^i TC + k_{Pout}^i R_P^{RO} - \mu_{RP}^i R_P, \#(3)$$

$$\frac{dTC}{dt} = k_1 R_P\left(Ribo_{tot}^i - TC\right) - k_2^i TC - k_{Pin}^i\left(1 - \frac{RC}{RC_{MAX}}\right)P_N TC - \mu_{TC}^i TC, \#(4)$$

$$\frac{dP_P}{dt} = k_2^i TC - k_c P_P, \#(5)$$

$$\frac{dL}{dt} = k_2^i TC - \mu_L L, \#(6)$$

$$\frac{dP_S}{dt} = k_c P_P - \mu_P^i P_s - N_{P_s}^i v_p, \#(7)$$

$$\frac{dP_N}{dt} = k_c P_P - k_{Pin}^i\left(1 - \frac{RC}{RC_{MAX}}\right)P_N TC - \mu_P^i P_N. \#(8)$$

With rate constant k_1 free host ribosomes form a translation complex TC with the viral plus-strand RNA genome R_P. The total number of ribosomes ($Ribo_{tot}^i$) available for viral RNA translation was assumed to be constant and the number of free ribosomes is given by $Ribo = Ribo_{tot}^i - TC$. Note that $Ribo_{tot}^i$ is only a fraction of the total cellular ribosome number. Translation of the viral plus-strand RNA genome generates the viral polyprotein P_P and luciferase L with rate constant k_2^i. The viral polyprotein P_P is subsequently cleaved with rate constant k_c into structural and non-structural viral proteins, P_S and P_N, respectively. The translation complex TC decays with rate constant μ_{TC}^i, while luciferase and viral proteins degrade with rate constants μ_L and μ_P^i, respectively. Note that for simplicity we assume structural and non-structural proteins degrade with the same rate constant, which has been summarized as one virus-specific viral protein degradation rate μ_P^i.

The subsequent processes of viral RNA synthesis in the replication organelle (RO) are modeled by Eqs. 9 to 13 representing the replicase complex RC, double-stranded RNA R_{DS}, a double-stranded RNA intermediate complex R_{IDS}, newly synthesized viral plus-strand RNA in the RO R_P^{RO}, and non-structural proteins within the RO, P_N^{RO}, as follows:

$$\frac{dRC}{dt} = k_{Pin}^{i}(1 - \frac{RC}{RC_{MAX}})P_{N}TC - k_{4m}^{i}RC + k_3 R_P^{RO} P_N^{RO} - \mu_{RO} RC, \#(9)$$

$$\frac{dR_{DS}}{dt} = k_{4m}^{i}RC - k_5 R_{DS} P_N^{RO} + k_{4p}^{i} R_{IDS} - \mu_{RO} R_{DS}, \#(10)$$

$$\frac{dR_{IDS}}{dt} = k_5 R_{DS} P_N^{RO} - k_{4p}^{i} R_{IDS} - \mu_{RO} R_{IDS}, \#(11)$$

$$\frac{dP_N^{RO}}{dt} = k_{4m}^{i}RC - k_3 R_P^{RO} P_N^{RO} - k_5 R_{DS} P_N^{RO} + k_{4p}^{i} R_{IDS} - \mu_{RO} P_N^{RO}, \#(12)$$

$$\frac{dR_P^{RO}}{dt} = k_{4p}^{i} R_{IDS} - k_3 R_P^{RO} P_N^{RO} - k_{Pout}^{i} R_P^{RO} - v_p - \mu_{RO} R_P^{RO}. \#(13)$$

Viral non-structural proteins recruit the viral RNA after translation to the replicase complex [58]. Hence, for viral RNA synthesis, we require translated viral RNA, i.e., the translation complex TC instead of free cytosolic viral RNA R_P to interact with the non-structural proteins. Thus, the translation complex TC together with a subset of non-structural proteins P_N are imported into the RO, where they lead to the formation of a replicase complex RC with rate constant k_{Pin}^{i}. Following successful replicase complex formation, ribosomes dissociate from the complex as is accounted for in Eq. (4). We furthermore assume that there is a limitation in the number of replicase complexes formed within a cell. To do so, we extend k_{Pin}^{i} by $(1 - \frac{RC}{RC_{MAX}})$ with the carrying capacity for replicase complexes RC_{MAX} [57,59].

Within the RO, minus-strand RNA synthesis occurs from the replicase complex with rate constant k_{4m}^{i}, leading to the formation of double-stranded RNA R_{DS}, which along with the non-structural proteins are released from the RO, P_N^{RO}. Subsequently, the double-stranded RNA binds again to P_N^{RO} with rate constant k_5 to form a double-stranded intermediate replicase complex R_{IDS}, initiating plus-strand RNA synthesis with rate constant k_{4p}^{i}. For simplicity, we assume that minus and plus-strand RNA synthesis occur with the same rate constant $k_{4m}^{i} = k_{4p}^{i}$. The newly synthesized plus-strand RNA genomes R_P^{RO} either remain within the RO to make additional replicase complexes with rate constant k_3, are exported out of the RO into the cytoplasm for further RNA translation with export rate k_{Pout}^{i}, or are packaged together with structural proteins into virions V_R and are subsequently released from the cell. Assembly

and release of virus particles is represented by a Michaelis-Menten type function v_p described below (Eq. 15, compare [55,60]). The RNA and protein species within the RO (RC, R_{DS}, R_{IDS}, R_P^{RO}, P_N^{RO}) are assumed to degrade with the same decay rate μ_{RO} and represent the decay of the entire replication organelle.

The released virus V_R may re-infect the same cell or infect new cells with rate constant k_{re}, or degrade with rate constant μ_V^i, resulting in the equation

$$\frac{dV_R}{dt} = v_p - k_{re}V_R - \mu_V^i V_R. \#(14)$$

Assembly of newly synthesized viral plus-strand RNA genome R_P^{RO} and viral structural proteins P_S into viral particles and their subsequent release from the host cell are described using a Michaelis-Menten type function, with rate

$$v_p = k_p R_P^{RO} \frac{P_S}{K_D^i N_{P_S}^i + P_S}, \#(15)$$

where k_p is the virion assembly and release rate and $k_p R_P^{RO}$ being the maximum release rate that is limited by viral resources. Let $N_{P_S}^i$ be the number of structural proteins in a virus of type i, then to produce virus at rate v_p will require a large number of proteins $K_D^i N_{P_S}^i$, where K_D^i is a scaling constant and $K_D^i N_{P_S}^i$ is the number that corresponds to the half-maximal release rate [see [55,60,61] for more details].

Pan-viral and virus-specific model parameters

To complete the model of the plus-strand RNA virus life cycle, we need to specify model parameters. To prevent overfitting and parameter uncertainty, we fixed many parameter values to either experimentally determined values or to values estimated in other modeling studies. In some cases, we were able to calculate rate constants directly, such as for viral RNA translation and synthesis, which could thus be fixed as described in S1 Supporting text. An overview of all parameters values is given in Table 2.

Parameter estimation, model selection, and model analysis

Our model has 61 parameters; 30 of them were fixed, while 31 were estimated by fitting the model to experimental data. As the fixed parameter values were experimentally measured, calculated, or taken from literature, we had information about which were virus specific (S1 Supporting text and Table 2). To determine which of the remaining model parameters are conserved across the different viruses considered (pan-viral) and which parameters are virus-specific, we performed several rounds of model evaluation using the Akaike information criterion (AIC) and model identifiability analysis (profile likelihood estimation). See S2 Supporting text for a description of the model selection process.

We fit the plus-strand RNA virus replication model simultaneously to the virus-specific data sets for HCV, DENV, and CVB3. To fit the mathematical model to the experimental data, we calculated the total plus-strand RNA $R_P^{tot} = (V_E + R_P + TC + RC + R_{DS} + R_{IDS} + R_P^{RO})$, total minus-strand RNA $R_M^{tot} = (R_{DS} + R_{IDS})$, luciferase L, and total infectious virus $V^{tot} = (V + V_R)$. Note that our model accounts for infectious virus since infectious titers were measured for all three viruses. Further note that for the infectious virus measurements for HCV, $V^{tot} = V_R$, since measuring infectious virus started 20 h pi. We introduced three scale factors f_L, f_{R_M}, and f_{R_P} to re-scale experimental measurements acquired in relative measurements (plus-strand RNA for DENV), molecules per cell (plus- and minus-strand RNA measurements for HCV and plus-strand RNA for CVB3) and relative light units (luciferase for DENV and CVB3).

We implemented the model in MATLAB (The MathWorks) 2016 using the Data2Dynamics toolbox [62]. We assessed model identifiability using the profile likelihood estimation method implemented in Data2Dynamics [62,63]. In Data2Dynamics, a parameter is identifiable if its 95% confidence interval is finite [62,63]. Note that an estimated model parameter may hit a predefined upper or lower parameter boundary which hampers the calculation of the 95% confidence interval. In such cases, a one-sided 95% confidence interval has been calculated starting from the estimated model parameter and thus with its upper or lower boundary marked with + in Table 2. Details about the model fitting and model selection process are in S1 Supporting material.

We performed a global sensitivity analysis in MATLAB using the extended Fourier Amplitude Sensitivity Test (eFAST) [64]. We calculated sensitivities with regard to the total plus-strand RNA (R_P^{tot}) concentrations throughout the course of infection. We studied hypothetical drug interventions by

382 including the effects of direct acting antivirals (DAA) into the model. For this purpose, we simulated
383 putative drugs targeting (1) viral entry and internalization k_e, (2) release of the viral RNA genome k_f, (3)
384 formation of the translation initiation complex k_1, (4) viral RNA translation k_2, (5) polyprotein cleavage
385 k_c, (6) replicase complex formation k_{Pin}, (7) minus- and plus-RNA synthesis k_{4m} and k_{4p}, as well as (8)
386 virus particle production and release (v_p). To introduce drug effects into the model, we assumed a drug
387 efficacy parameter $0 \leq \varepsilon \leq 1$, and multiplied the parameters above by $(1 - \varepsilon)$ to simulate drug
388 treatment. Similar to our previously published DENV model, we calculated the average virus particle
389 concentration released from the cell upon drug administration ($\varepsilon \neq 0$) until 5 days post drug
390 administration, i.e., a drug treatment observation window of 120 h. The average virus particle
391 concentration with treatment ($\varepsilon \neq 0$) has been normalized to the average virus concentration without
392 drug treatment ($\varepsilon = 0$). Note that we studied two different time points of drug administration: at the
393 very beginning of the infection, 0 h pi, and when the system is in steady state, 100 h pi.
394

395 Results

396 As shown in Fig 2 (left panels), the model replicates the experimental data for all three viruses. The
397 comparison of their plus-strand RNA and virus (infectious particles) dynamics, reveals virus-specific
398 characteristics. CVB3 is fast-replicating with a life cycle of about 8 hours (depending on the cell type)
399 after which the infected cells begin to die. Similarly, DENV is also cytopathic but seems to be slower
400 replicating and thus has a longer life cycle than CVB3 with infectious particles being produced at about
401 16 h pi [56]. In contrast, HCV is non-cytopathic with a much longer life cycle. In our experimental
402 measurements, the CVB3 viral load peaked at 8 h pi with 193 PFU/mL/cell. The HCV viral load peaked
403 with 0.06 PFU/mL/cell around 44 h pi, while the DENV viral load reached its maximum with
404 approximately 8 PFU/mL/cell around 10 hours earlier at 30 to 34 h pi (Fig 2A, 2B, 2C). We calculated the
405 corresponding average virus concentration per measurement time point for HCV, DENV, and CVB3 per
406 cell as 0.04 PFU/mL/cell, 1.8 PFU/mL/cell, and 40 PFU/mL/cell, respectively. Thus, the average infectious
407 HCV viral load was only 4% of the average DENV viral load and only 0.3% of the average CVB3 viral load.
408 Similarly, CVB3 reached a peak of almost 500,000 plus-strand RNA copies per cell at 8 h pi, while HCV
409 produced only 10,000 copies per cell at 70 h pi, i.e., 98% less than CVB3.

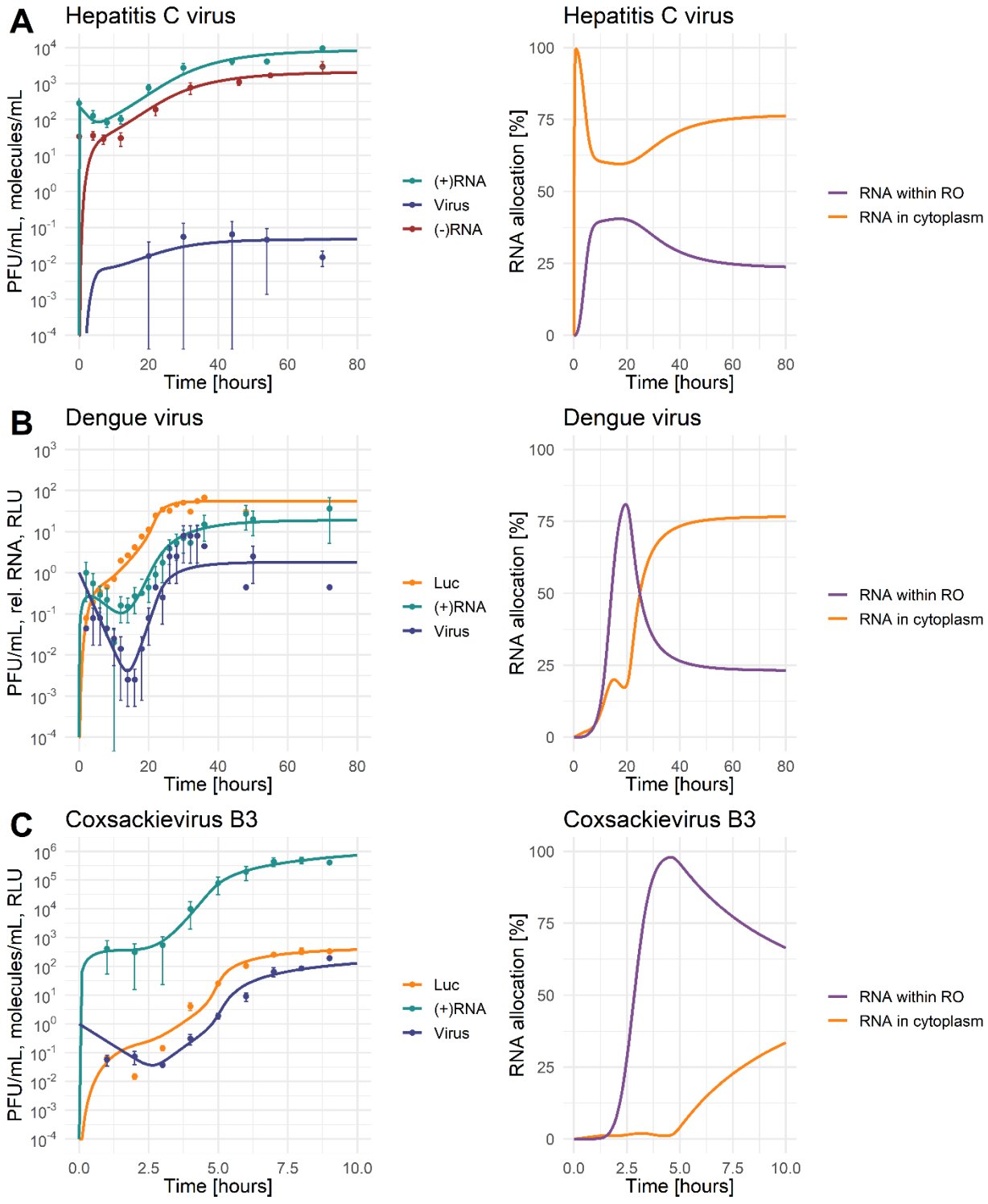

Figure 2: Best model fit (solid line) to the data with standard deviation (left) and model prediction of plus-strand RNA allocation between cytoplasm and replication organelle (RO) (right). For parameter values see Table 2. [LEFT: green: (+)RNA = $R_P^{tot} = (V_E + R_P + TC + RC + R_{DS} + R_{IDS} + R_P^{RO})$, red: (-

)RNA = $R_M^{tot} = (R_{DS} + R_{IDS})$, blue: A) and B) Virus = $V^{tot} = (V + V_R)$ or C) Virus = $V^{tot} = V_R$, yellow: Luc = L; RIGHT: yellow: RNA in cytoplasm = $(R_P + TC)/R_P^{tot}$, purple: RNA within replication organelle (RO) = $RC + R_{DS} + R_{IDS} + R_P^{RO})/R_P^{tot}$; Infectious virus in PFU/mL, (+) and (-)RNA were measured in molecules/mL or relative RNA concentration, luciferase was measured in relative light unit (RLU)]

Model selection and uncertainty

The intracellular model structure has been taken from our previously published HCV model [19], upon which we built with our recently published DENV model [55]. However, a striking difference from our previous HCV and DENV models is the absence of host factors involved in replicase complex formation and/or virus assembly and release. We have previously shown that host factors are recruited by the virus and seem to be beneficial for host cell permissiveness and virus replication efficiency [19,55]. Instead, here we describe inter-viral replication differences with virus-specific parameter sets based on model evaluation by AIC and profile likelihood estimation (see Methods, S1 and S2 supporting texts).

Including the maximal number of replicase complexes (RC_{MAX}) improved the basic model AIC from 3025 to 1982 and thus served as a starting point for the virus specific model selection process (see S1 Supporting material). After several rounds of model selection by comparing AICs and taking model identifiability into account, we added five virus specific processes to our basic model (from a total of 13 considered processes): (1) the total number of ribosomes $Ribo_{tot}^i$ available for viral RNA translation, (2) virus entry k_e^i, (3) viral genome release k_f^i, (4) formation of the replicase complex k_{Pin}^i, and (5) export of viral RNA from the RO into the cytoplasm k_{Pout}^i. Note that based on literature data and previous assumptions, we fixed some virus-specific and pan-viral processes and degradation rates (see S1 Supporting text and Table 2). The best-fit model showed high similarity to the virus-specific experimental measurements and a high degree of model identifiability (see Fig 2 for best fit, Fig 3 for the parameter profiles based on the profile likelihood estimation, and Table 2 for parameter values with 95% confidence intervals).

*Table 2: Parameter values and 95% confidence intervals in (). Note that parameter values marked with * were fixed due to previous assumptions and calculations. Furthermore, confidence intervals marked with*

443 *+ hit the set estimation boundary; ± calculated from the data; # experimentally measured for Zika virus; ‡*
444 *experimentally measured for poliovirus.*

Parameter	Description	HCV	DENV	CVB3	Unit
k_e^i	Virus entry rate	10 (1.9, *10*$^+$)	0.31 (0.28, 0.34)	1.3 (0.9, 1.7)	1/h
k_f^i	RNA release rate	10 (1.7, *10*$^+$)	0.008 (0.006, 0.01)	0.016 (0.006, 0.04)	1/h
k_1	Formation rate of the translation complex	1000 (840, *1000*$^+$)			mL/molecule h
k_2^i	Virus RNA translation rate	180 [65]	100 [55]	300 ‡ [66]	1/h
k_c	Polyprotein cleavage rate	2.24 (1.18, 7.4)			1/h
k_3	Formation of additional replicase complexes within the replication organelle	42 (5.5, 525)			mL/molecule h
$k_{4m}^i = k_{4p}^i$	Minus- and plus-strand RNA synthesis rate	1.1 [65]	1.0 [55]	50 ‡ [66]	1/h
k_{Pin}^i	Formation rate of the replicase complex	4.4 (2.4, 7.5)	0.45 (0.29, 0.74)	1.4 (0.52, 4.09)	mL/molecule h
k_5	Formation rate of the replication intermediate complex	6018 (1549, 68401)			mL/molecule h
k_{Pout}^i	Export rate of viral RNA out of the replication organelle	33 (0.8, 1477)	53 (16, 432)	0.23 (0.16, 0.43)	1/h
k_p	Assembly and release rate	158 (47, *1000*$^+$)			mL/molecule h
k_{re}	Reinfection rate	0.01 (*0.01*$^+$, 0.038)			1/h
μ_{RP}^i	Degradation rate of cytosolic viral RNA	0.26 [65]	0.23 [67]	0.15 ‡ [68]	1/h
μ_{TC}^i	Degradation rate of the translation complex	0.13 *	0.115 *	0.075 *	1/h
μ_{RO}	Degradation rate of viral RNA and protein within the replication organelle	0.086 [19]			1/h
μ_P^i	Degradation rate of viral protein	0.08 [19]	0.46 [67]	0.43 [69]	1/h
μ_L	Degradation rate of luciferase	0.35 [19]			1/h

μ_V^i	Degradation rate of extracellular infectious virus	0.1 [57]	0.13 [70]	0.08 [71,72]	1/h
μ_{VE}	Degradation rate of intracellular virus within the endosome		0.23 # [73]		1/h
V_0^i	Initial virus concentration	0.2 (0.16, 0.25)	1 (0.8, 1.3)	1 (0.4, 2.2)	molecules/mL
$Ribo_{tot}^i$	Total ribosome concentration	0.005 (0.004, 0.007)	0.48 (0.41, 0.55)	6.7 (5.0, 9.1)	molecules
RC_{MAX}	Maximum number of replicase complexes		0.46 (0.34, 0.64)		molecules/mL
K_D^i	Scaling constant for virus	0.04 ±	1.8 ±	40 ±	virions
$N_{P_S}^i$	Number of structural proteins needed to produce 1 virion	180 [65,74]	180 [55,74]	60 [15]	molecules/virion
$f_{R_P}^i$	Scale factor for plus-strand RNA	394 (274, 524)	0.76 (0.58, 1.0)	550 (245,1366)	
$f_{R_M}^i$	Scale factor for minus-strand RNA	1377 (945, 1872)	-	-	
f_L^i	Scale factor for luciferase	-	0.41 (0.33, 0.5)	0.08 (0.06, 0.1)	

445

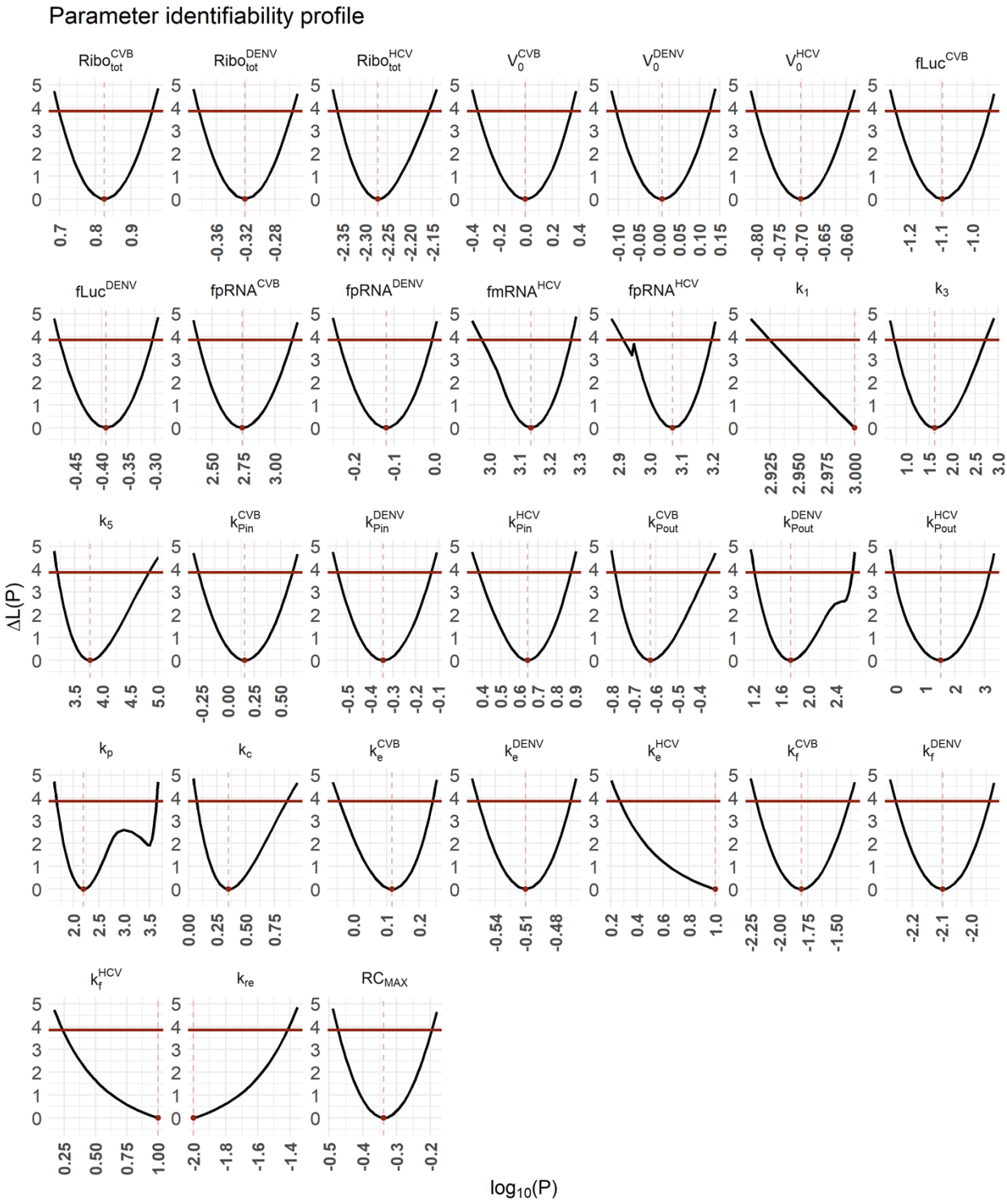

Figure 3: Uncertainty analysis of the best-fit model. For parameter values and 95% confidence intervals see Table 2. The best fit is shown in Fig. 2.

RNA allocation

The allocation of plus-strand RNA in the cytoplasm and within the RO, as predicted by our model, shows interesting virus-specific differences (Fig 2 right panel). Compared to the total amount of viral RNA, HCV has most of the RNA allocated to the cytoplasm and thus available for viral RNA translation at any given time. In DENV, our model predicted that the allocation strategy changes throughout the viral life cycle, with the majority of plus-strand RNA within the RO initially. At around 25 h pi, viral RNAs are equally distributed between the two compartments, while at the end of the DENV life cycle the majority of viral RNA is in the cytoplasm. Interestingly, at steady state, the predicted allocation of both HCV and DENV is the same, with 25% of RNA allocated to the RO and 75% to the cytoplasm. In contrast, the predicted viral RNA allocation is opposite for CVB3. CVB3 has the majority of RNA available within the RO, which contributes to the 2 to 3 log higher viral load.

Virus specificity

For a successful virus infection, the first hurdles to overcome are virus entry and the release of the viral genome into the cytoplasm. The rate constants for virus entry k_e^i and vRNA release k_f^i had the highest estimated values for HCV. However, both values were practically non-identifiable suggesting a limitation in the amount of data. Hence, we could only estimate the lower boundary of the 95% confidence intervals, which suggest $k_e^{HCV} \geq 1.9\ h^{-1}$ and $k_f^{HCV} \geq 1.7\ h^{-1}$. CVB3 seems to be slightly better adapted to the cell line with a 4-times higher entry rate and 2-times higher vRNA release rates compared to DENV. According to our model selection process, the degradation rate of internalized virus within endosomes μ_{VE} was pan-viral suggesting neither an advantage nor disadvantage for the studied viruses.

The next processes in the viral life cycle are vRNA translation and polyprotein processing with parameters k_1 for the formation of the translation initiation complex, k_2^i vRNA translation, and k_c polyprotein cleavage. Models including virus-specific k_1 or k_c either did not improve the quality of the model fit (no AIC improvement) or were non-identifiable when tested as virus-specific and thus have been selected as pan-viral (see S2 Supporting material). However, the viral RNA translation rate k_2^i was calculated based on genome size and ribosome density and set as virus-specific (see S1 Supporting text). In the vRNA translation and polyprotein processing step, the only parameter our model selected as virus specific was the total number of ribosomes $Ribo_{tot}^i$. Since the ribosome number has been selected in the first round of model selection (see S2 Supporting text), it emphasizes the importance of this host factor

with CVB3 showing the highest estimated ribosome number available for RNA translation. In contrast, HCV and DENV use only 0.07% and 7% of the ribosomes CVB3 uses, respectively. Interestingly, increasing the number of ribosomes in the HCV life cycle to those of CVB3 (from $Ribo_{tot}^{HCV} = 0.005$ to $Rib o_{tot}^{HCV} = 6.7$ molecules per ml) increases the infectious virus load by three orders of magnitude (Fig 4A). In the same way, decreasing the number of ribosomes in the CVB3 life cycle to those of HCV (from $Rib o_{tot}^{CVB3} = 6.7$ to $Ribo_{tot}^{CVB3} = 0.005$ molecules per ml) decreases the CVB3 virus load by three orders of magnitude (Fig 4B). In contrast, when increasing the viral RNA synthesis rates of HCV to those of CVB3 (from $k_{4m}^{HCV} = k_{4p}^{HCV} = 1.1$ to $k_{4m}^{HCV} = k_{4p}^{HCV} = 50\ h^{-1}$), the viral load did not increase. However, decreasing the viral RNA synthesis rates of CVB3 to those of HCV (from $k_{4m}^{CVB3} = k_{4p}^{CVB3} = 50$ to $k_{4m}^{CVB3} = k_{4p}^{CVB3} = 1.1$ h^{-1}) decreased the viral load by one order of magnitude. This suggests an important role of ribosomes as key players in the production of structural and non-structural proteins necessary for efficient vRNA replication and virus production.

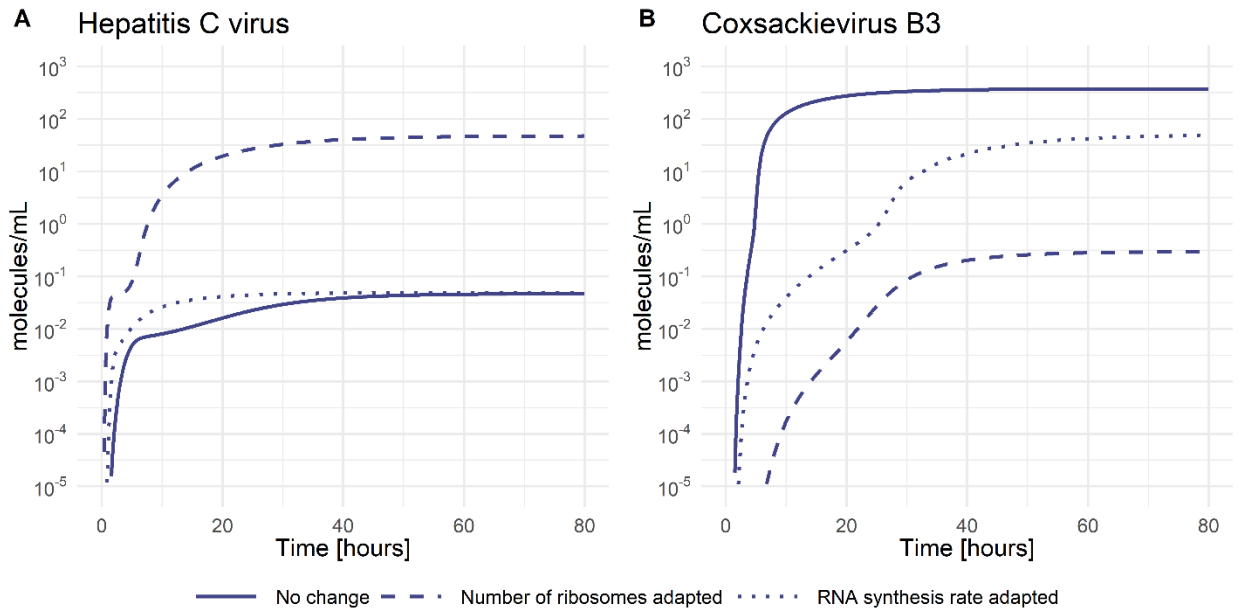

Figure 4: Infectious virus concentration with parameter adjustments. ***A)*** *HCV concentration with estimated parameters (solid), the number of ribosomes taken from CVB3 (dashed), and the RNA synthesis rate taken from CVB3 (dotted).* ***B)*** *CVB3 concentration with estimated parameters (solid), the number of ribosomes taken from HCV (dashed), and the RNA synthesis rate taken from HCV (dotted).*

The subsequent processes of vRNA replication depend on successful viral protein production. Viral non-structural proteins are crucial for the formation of the replicase complex and its formation rate k_{Pin}^{i}, which has been selected as virus specific. Here, HCV seems to be more efficient and better adapted to the Huh7 cell line, showing a 10- and 4-times faster formation rate compared to DENV and CVB3, respectively. Furthermore, our estimated replicase complex formation rates suggest that the formation of double membrane vesicles may be more efficient (HCV and CVB3) compared to the formation of invaginations (DENV). However, the maximum number of replicase complexes RC_{MAX} as well as the degradation of species within the RO (μ_{RO}) were not selected as virus-specific, especially since the viral RNA synthesis rates were initially set as virus-specific (Table 2). Interestingly, even though being a pan-viral model parameter, not all viruses reached the maximal number of replicase complexes RC_{MAX} (the carrying capacity). The dynamics of replicase complexes shows a clear separation between DENV and CVB3 versus HCV (Fig. 5A and 5B). CVB3 reached the estimated carrying capacity around 5 h pi, while DENV reached 98% of the possible carrying capacity around 25 h pi. Strikingly, the replicase complex formation for HCV reached its maximum at a 74% lower level of the pan viral carrying capacity, even though our model estimated the fastest RC formation rate for HCV.

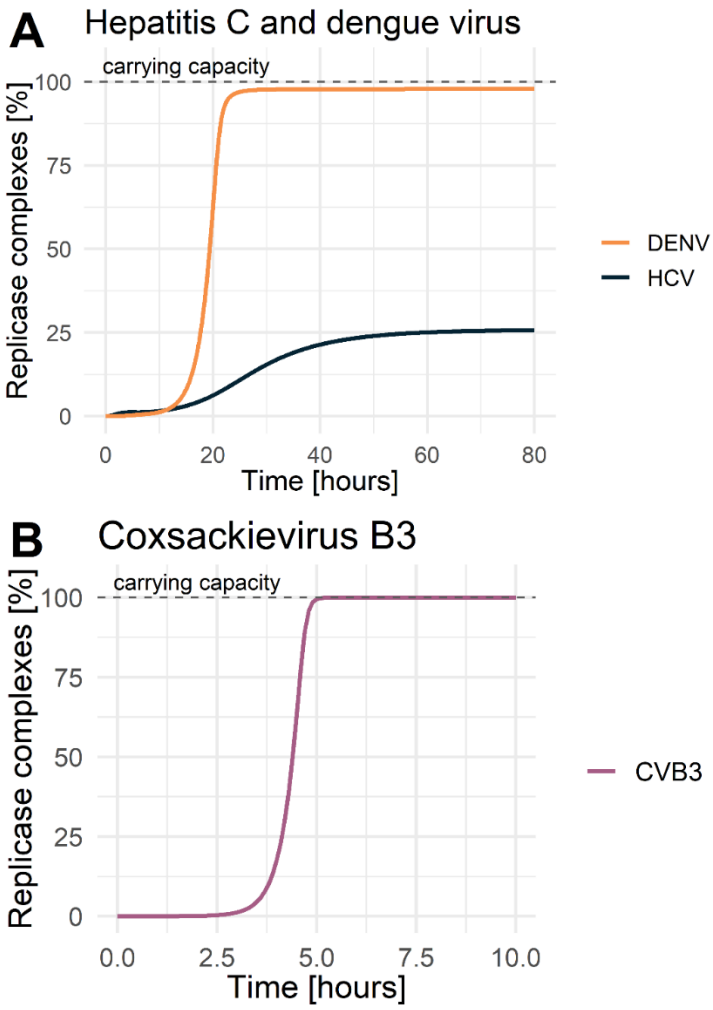

*Figure 5: Replicase complexes over time. Dynamics of replicase complexes for **A)** hepatitis C and dengue virus, **B)** coxsackievirus B3. The dashed grey line represents the carrying capacity or the maximum number of formed replicase complexes.*

The export of viral RNA from the RO to the site of RNA translation k^i_{Pout} has also been selected as virus specific, where HCV and DENV seem to be more efficient than CVB3 which showed an almost 190 times slower trafficking process.

Following the production of viral proteins and RNA genomes, the single components assemble into virions and are released from the cell. Here, the virus assembly and release rate k_p as well as the reinfection rate k_{re} have been selected as pan-viral, while the scaling constant K^i_D as well as the number

of structural proteins necessary per virion $N_{P_S}^i$ were calculated from the data or taken from the literature, respectively, and thus set as virus-specific (Table 2).

Sensitivity analysis and drug intervention

Having a detailed model of the intracellular replication of plus-strand RNA viruses, we next addressed the question of which processes shared across all viruses showed the highest sensitivity index to potential drug interventions (Fig 6). Our sensitivity analysis suggests that model parameters associated with vRNA translation (k_2^i) and synthesis within the RO (k_{4m}^i and k_{4p}^i) are highly sensitive for all viruses. Furthermore, all viruses were sensitive to the formation of replicase complexes k_{Pin}^i and its maximum number RC_{MAX}.

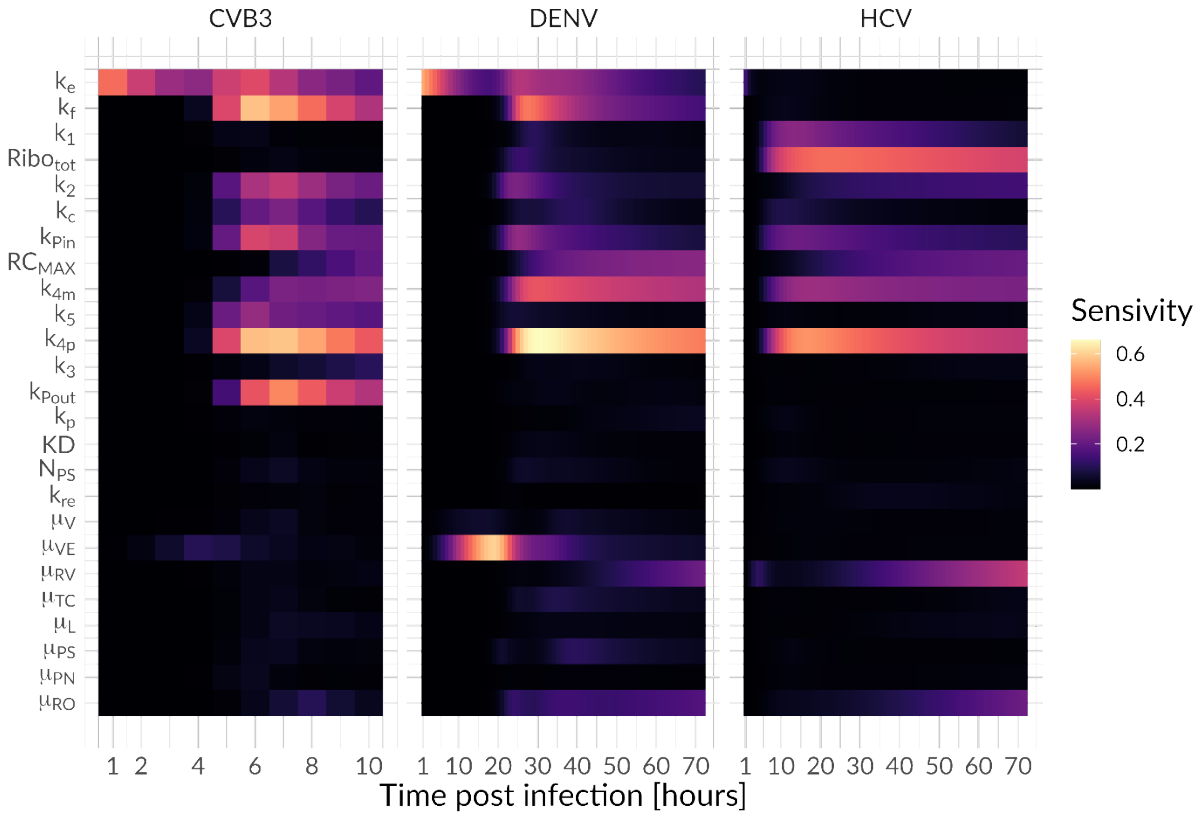

Figure 6: Global sensitivity profile for the model species plus-strand RNA over the course of infection (CVB3 = 10 hours, HCV = DENV = 72 hours).

Interestingly, over the course of infection, DENV and CVB3 showed a time-dependent sensitivity pattern beginning with viral entry (k_e^i) being sensitive, followed by the release of the viral genome (k_f^i). However, both model parameters were not sensitive for HCV, possibly due to practical non-identifiability (see above). Moreover, vRNA translation and replication seem to start around 5 or 20 h pi in CVB3 and DENV, respectively, suggesting viral entry as a rate limiting process.

There are also some interesting differences between the three viruses. While the formation of the translation initiation complex (k_1) showed a higher sensitivity in HCV, vRNA translation (k_2^i) was more sensitive for CVB3 and DENV. Furthermore, for HCV, the number of ribosomes available for HCV RNA translation was one of the most sensitive parameters, while having negligible sensitivity for CVB3 and DENV. This may be a reflection of the strength of the IRES (CVB3) or the 5' UTR/Cap (for DENV), where a strong IRES may require less ribosomes for robust recruitment to initiate vRNA translation. However, for CVB3 viral RNA export k_{Pout}^i is among the most sensitive processes, while being not sensitive for HCV and DENV. Interestingly, the degradation of virus in endosomes (μ_{VE}) showed the highest sensitivity among the degradation rates for DENV early in infection (around 10 to 25 h pi), while the degradation of cytosolic vRNA (μ_{RP}) seem to be highly sensitive towards the end of infection for both DENV and CVB3.

As a next step, we aimed to analyze if any processes can be targeted leading to a 99% reduction in extracellular virus upon inhibition. We therefore studied the effects of inhibiting core processes of the viral life cycle (Fig 7). We then simulated *in silico* the administration of a hypothetical drug at two different time points using our mathematical model: at the very beginning of the infection (0 h pi) or at steady state (100 h pi). For all viruses and both drug administration time points, we determined the critical drug efficacy, ε, where the viral life cycle is successfully inhibited and the *in-silico* infection is cleared. Note that we define a virus infection as being cleared if extracellular virus is reduced by more than 99%. By testing both drug administration time points, we found that at the beginning of infection (0 h pi) inhibiting any process led to an eradication of the virus (Fig 7). Since the viral replication machinery is not established, viral entry and vRNA release may be possible drug targets, however, an almost 100% inhibition ($\varepsilon \sim 1$) was necessary to block the infection process (S1 Table). Obviously, *in-silico* drugs targeting virus entry and vRNA release at a time point after an established viral infection, is not able to reduce the viral load. However, for both drug administration time points, targeting vRNA translation as well as vRNA synthesis showed the strongest effect, and thus are the most promising drug targets (S1 Table). Interestingly, targeting the formation of the replicase complexes could not clear (or

574 even reduce) CVB3 infection with a drug administration given at steady state (S1 Table). Moreover, in
575 the case of DENV, targeting vRNA export from the RO into the cytoplasm at steady state led to a 6%
576 increase in virus with incomplete inhibition. Only a 100% inhibition and thus a drug efficacy of 1 was
577 able to clear the virus by 99%.
578

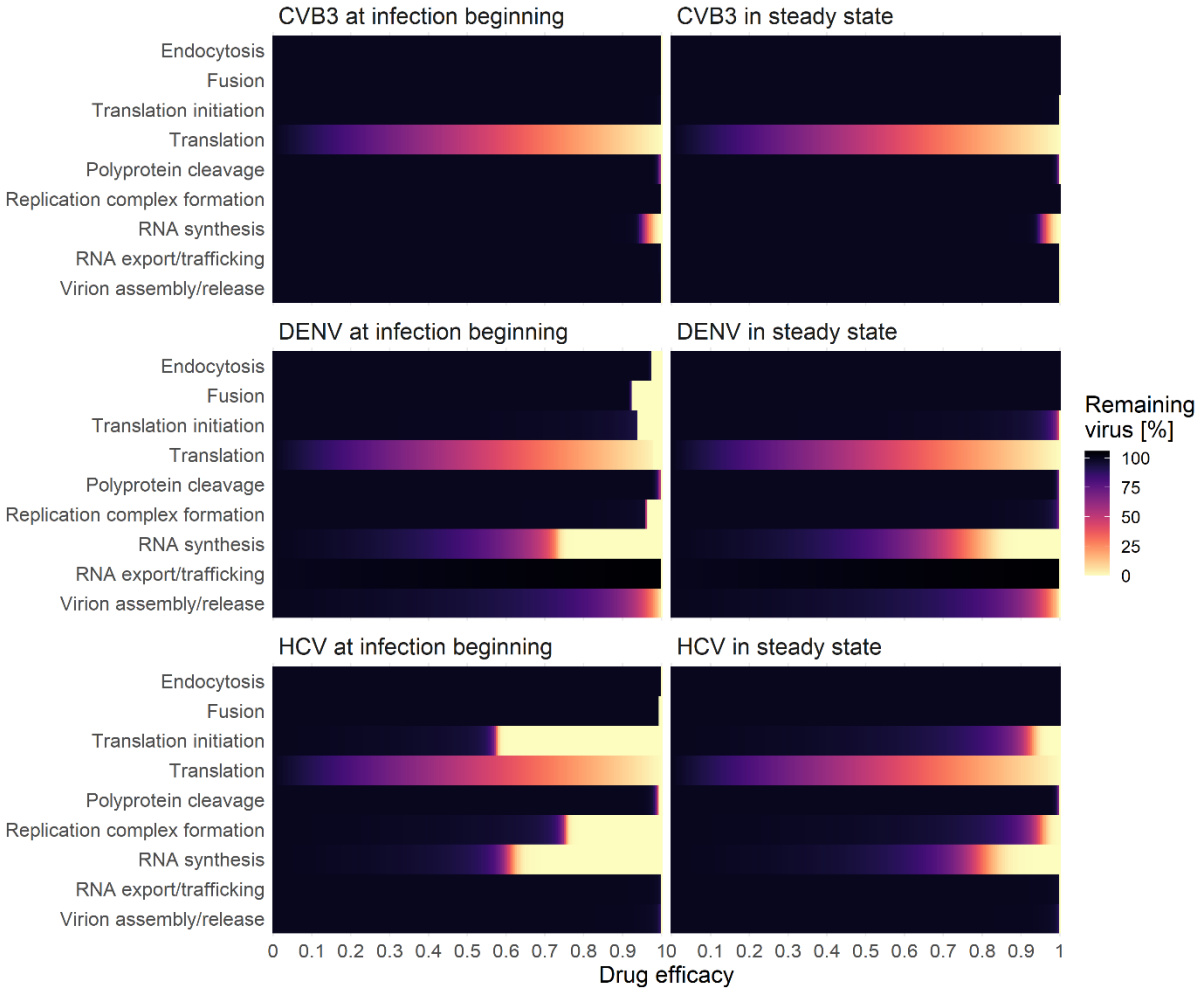

579

580 *Figure 7: Effects of drug interventions at two different time points: at infection beginning (left) and in*
581 *steady state (right). A successful drug treatment leads to a more than 99% viral eradication (light*
582 *yellow), while an ineffective drug treatment leads to 100% remaining virus (black).*

583

584 Since most direct acting antiviral drugs are highly efficient in combination, we determined the critical
585 drug efficacy of individual drugs inhibiting either translation complex formation, vRNA translation, or

polyprotein cleavage used in combination with drugs that inhibit vRNA synthesis or formation of the replicase complex at steady state (Figs 8 and 9 and S1 and S2, Figs, S1 Table). We identified the "sweet spot" for efficient viral eradication (by more than 99%). Our model predicted that HCV and DENV showed a comparable pattern of viral clearance to a combination of two drugs, while for the clearance of CVB3 higher drug efficacies were necessary to clear the infection. Inhibiting vRNA synthesis in combination with vRNA translation or polyprotein cleavage by more than 90% was an efficient combination for HCV and DENV (Fig 8B and 8C, S1 Table, S2A Fig). However, to clear the infection in all viruses, vRNA synthesis and translation or polyprotein cleavage, have to be inhibited by more than 99% or 98%, respectively (Figs 9B and 9C). Interestingly, inhibiting vRNA synthesis and translation complex formation by more than 76% showed the overall lowest critical drug efficacy to clear an HCV infection. Nevertheless, for CVB3, the vRNA synthesis and translation complex inhibition need to be higher than 99.3% to clear the infection with an almost 10 hours delay in viral clearance (Figs 8A and 9A, S1 Table). Overall, we found the lowest pan-viral critical drug efficacy was for the combined inhibition of vRNA synthesis and polyprotein cleavage with a required 98% effectiveness for each drug (Figs 8C and 9C, S1 Table,). Note that we also tested *in silico* the combination therapy of inhibiting translation complex formation, vRNA translation, and polyprotein cleavage together with replicase complex formation. However, higher critical drug efficacy constants were needed to clear the infection (S1, S2 Figs and S1 Table).

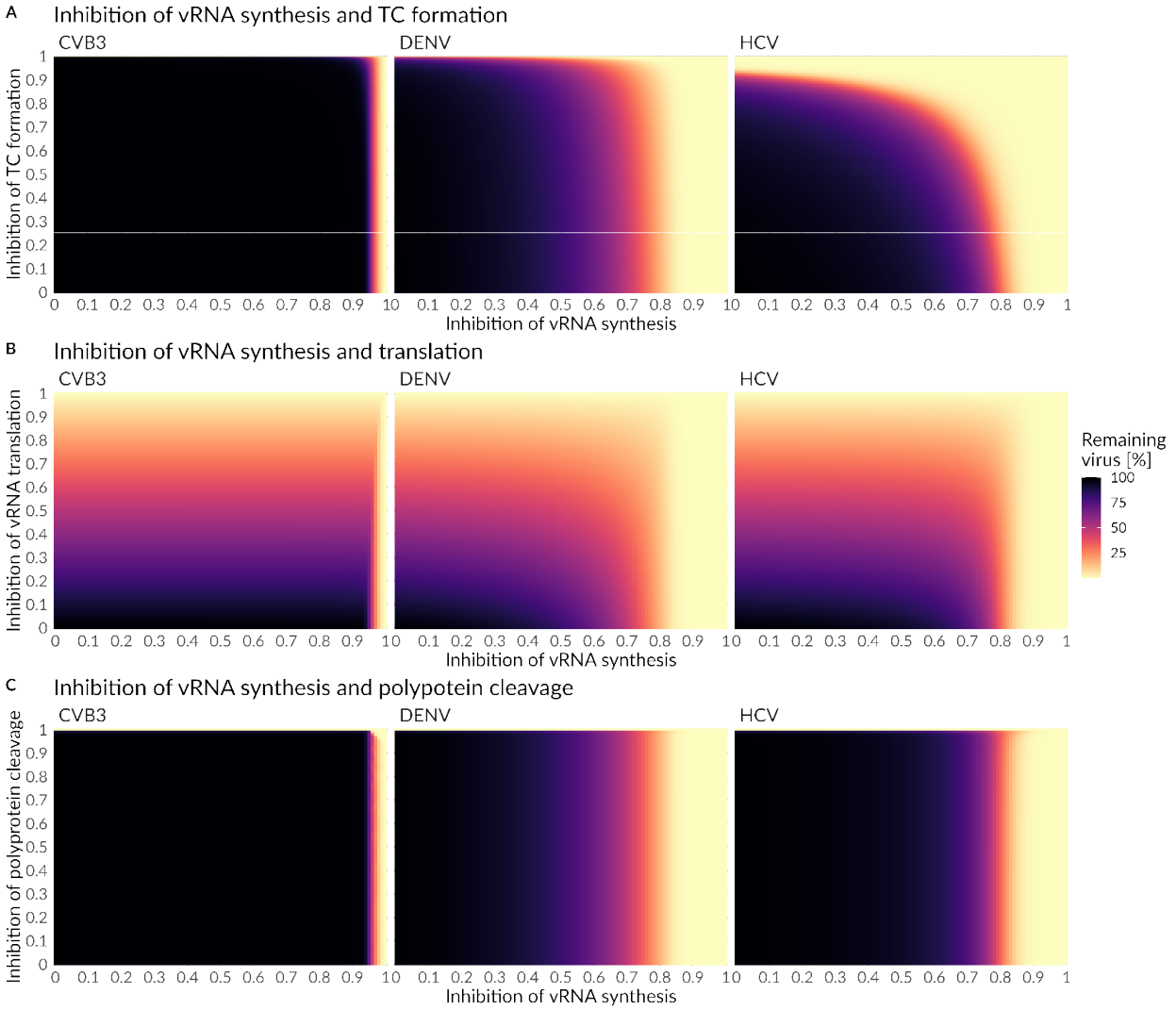

*Figure 8: Combined drug effects on **A)** vRNA synthesis and formation of translation complex (TC), **B)** vRNA synthesis and translation, and **C)** viral RNA synthesis and polyprotein cleavage. Initiation of treatment was in steady state (100 h pi). A successful drug treatment leads to more than 99% viral eradication (light yellow), while an ineffective drug treatment leads to 100% remaining virus (black).*

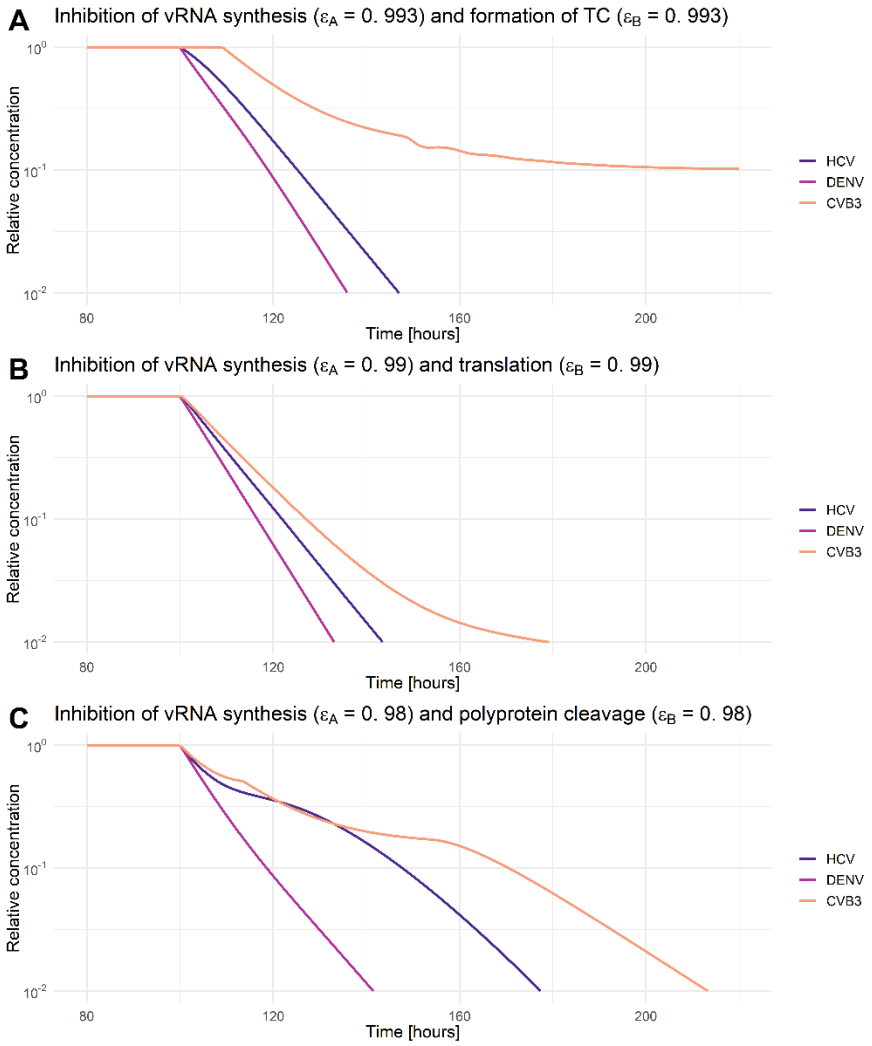

*Figure 9: Relative virus decay under combination therapy that clears HCV, DENV, and CVB3 infections. A combined drug effect on **A)** vRNA synthesis and formation of translation complex (TC), **B)** vRNA synthesis and translation, and **C)** viral RNA synthesis and polyprotein cleavage. Initiation of treatment was in steady state (100 h pi). The drug efficacy constant (ε_A and ε_B) were chosen as minimal efficacies to clear all three viruses. For comparability, virus-specific concentrations in steady state have been normalized to their virus-specific pre-treatment steady state concentration. A successful drug treatment leads to a more than 99% viral eradication (light yellow), while an ineffective drug treatment leads to 100% remaining virus (black).*

Discussion

Mathematical modeling of viral dynamics has a long history and has been applied to a variety of viral infectious diseases [25]. Population based models considering susceptible and infected cell populations,

623 especially studying virus-host interactions and treatment opportunities for HIV, HCV and Influenza,
624 represent the most prominent mathematical models in the field [25,75–78]. However, mathematical
625 models considering intracellular viral replication mechanisms in detail are still limited and are usually
626 developed for one specific virus such as HCV [19,57,59,79,80], DENV [55], HIV [81], or influenza A virus
627 [60,61,82–87]. Recently, Chhajer et al (2021) studied with a simplified mathematical model the viral life
628 cycles of the plus-strand RNA viruses HCV, Japanese encephalitis virus, and poliovirus. The authors
629 mainly focused on the slow and delayed kinetics of the intracellular formation of replication organelles,
630 which may predict infection outcome [88]. To our best knowledge, we present here the first
631 mathematical model that studies simultaneously the complexity of intracellular viral replication kinetics
632 for three different representatives of plus-strand RNA viruses, namely HCV, DENV, and CVB3, measured
633 in the same cell line – Huh7. The basis for our present study were our previously published intracellular
634 models for HCV [19,57] and DENV [55], which we generalized and adapted to reflect the intracellular
635 replication mechanisms of plus-strand RNA viruses more broadly, as well as the underlying experimental
636 conditions. We compare viral replication mechanisms as well as pan-viral similarities and virus-specific
637 differences, which may help to understand acute or chronic infection outcome that in turn may be an
638 initial step towards the development of broad-spectrum antiviral treatment strategies.
639
640 Our best-fitting model showed high similarity with the virus-specific data and a high degree of
641 parameter identifiability. However, it showed one shortcoming in capturing the dynamics of the
642 experimental measurements of virus in DENV: the viral peak and subsequent drop of the extracellular
643 DENV concentration around 32 h pi. However, in our previously published DENV model, we showed that
644 the dynamics of extracellular infectious virus was dependent on host factors that were packaged into
645 the virions [55]. Since we did not include host factors into the current model, except for ribosomes, our
646 aim was to describe the average extracellular virus dynamics for the first 25 h pi. In the final model, we
647 estimated 31 parameters of which 27 were identifiable. The 95% confidence intervals of four parameter
648 values hit the upper or lower boundary of estimation, where changing of the parameter boundaries by
649 up to 1000-fold did not lead to an improvement of the model fit or to improved identifiability.
650
651 The non-identifiable rate constant of the naïve cell infection k_{re} may be explained by the fact that
652 reinfection in our culture system may not occur for each virus. However, the process remained in the
653 final model because of different MOI infection experiments, where a lower MOI (MOI of 1 as in the case
654 of CVB3 and HCV) may account for multiple rounds of infection. The formation rate of the translation

initiation complex k_1 seems to be a non-identifiable process in the model structure, as it was also non-identifiable in our previous DENV model [55]. Further, the model processes of virus entry and vRNA genome release, k_e and k_f, were practically non-identifiable for HCV. A possible explanation for both processes being non-identifiable may be insufficient experimental measurements for HCV to uniquely estimate both rate constants, e.g., the lack of intracellular protein concentration measurements for HCV. However, since both parameters were identifiable for CVB3 and DENV and both processes were selected as virus-specific, k_e^{HCV} and k_f^{HCV}, they remained virus-specific in the final model.

Virus specific differences and pan-viral similarities

Studying similarities and differences in the viral RNA translation and replication strategies of different viruses is experimentally challenging. Our mathematical model may help to shed light on this topic by studying 25 processes from cell infection to release of the newly packaged infectious virions. Five processes within the viral life cycle were determined to be virus-specific: (i) virus entry, (ii) release of vRNA genome, (iii) the number of ribosomes available for vRNA translation, (iv) formation of replicase complexes, and (v) trafficking of newly produced viral genomes from the RO into the cytoplasm.

Virus internalization and genome release: The three viruses we studied each have different internalization processes mediated by differences in attachment/entry versus uncoating receptors [89]. HCV replicates *in vivo* in hepatocytes and consequently HCV showed the most efficient internalization and genome release processes in our studied hepatocyte derived Huh7 cells. *In vitro,* HCV replicates most efficiently in Huh7 cells and its closely related sub-clones, while the infection of other cell lines has been challenging [90]. However, both DENV and CVB3 have a broad tropism. DENV infects monocytes, macrophages, and dendritic cells and CVB3 infects brain and cardiac tissue as well as hepatocytes [15,35,91–93]. Thus, the faster internalization and genome release of CVB3 in comparison to DENV, and thus its ability to replicate very well in Huh7 cells, is not surprising due to its broader cellular tropism.

Viral RNA translation: Among the plus-strand RNA viruses we studied, CVB3 represents the fastest replicating virus with a life cycle of around 8 to 10 hours. Newly synthesized CVB3 RNA is detectable at two h pi in the Golgi apparatus, the site of ROs and thus vRNA synthesis. Levels of viral RNA increase rapidly and peak four h pi [94]. One key feature of successful CVB3 RNA replication is its ability to shut off host mRNA translation, carried out by the virus by degrading eukaryotic initiation factor eIF4G

important for the cellular cap-dependent translation complex formation. The result is not only the rapid availability of non-structural proteins required for replicase complex formation [95], but also a lower level of components of the cell's intrinsic immune response. Interestingly, we found the highest total ribosome availability for CVB3, in agreement with its ability to shut-off the translation of the host's mRNA while keeping vRNA translation high due to a very efficient internal ribosome entry site (IRES). According to our calculated viral RNA translation rate constants, translation is 2 to 3 times faster compared to HCV and DENV, respectively. It has been shown that the polysome size – the number of ribosomes bound to a single CVB3 RNA molecule, which translate the viral genome at the same time – is around 30 ribosomes per polysome, but changes over the course of the CVB3 life cycle; 40 ribosomes per polysome at the beginning of the CVB3 life cycle and 20 ribosomes later in infection [66,96]. Furthermore, Boersma et al. (2020) found that CVB3 translation rates were independent of host translation shup down. However, the authors speculated that a host translation shut down may boost the CVB3 translation at the end of its life cycle where host cell resources may be limited [97]. Conversely, for DENV it has been shown that the DENV RNA template is only sparsely loaded with ribosomes and showed a low translation efficiency [98]. Nevertheless, Roth et al. (2017) found that the host's mRNA translation decreases during DENV infection, suggesting that DENV also has the ability to repress the host mRNA translation although not as efficiently as CVB3 [23]. A partial host cell RNA translation shut-off and consequently a higher number of ribosomes available for DENV RNA translation is predicted by our model, with DENV having the second highest predicted ribosome concentration. Interestingly, even though DENV is able to partially shut down the host's mRNA translation, this suppression does not seem as efficient compared to the complete CVB3 host shut-off.

Formation of the replicase complex: Our model suggests a faster formation of double membrane vesicles compared to invaginations, i.e., HCV and CVB3 showed faster replicase complex formation compared to DENV. Compared to DENV and CVB3, HCV showed a 10- and 4-times faster rate of replicase complex formation, respectively. A possible reason may be cell tropism with hepatocellular-derived Huh7 cells being the cell line of choice for studying HCV. Interestingly, the host mRNA translation shut-off of CVB3 was not associated with a faster supply of non-structural proteins (RdRp) and thus faster replicase complex formation. However, host cell translation shut off may be associated with higher availability and more efficient utilization of viral resources for the formation of replicase complexes, as suggested by our model. CVB3 reached the maximal number of replicase complexes after around 5 h pi, while HCV used 76% less of the possible cell's carrying capacity. However, cell tropism and thus a

specific set of host factors involved in the process of replication organelle and replicase complex formation may be the crucial factors in this process, as we have shown previously for HCV and DENV [19,55].

Viral RNA export from the RO into the cytoplasm: A striking difference between *Flaviviridae* (HCV and DENV) and *Picornaviridae* (CVB3) concerns the parameter values and model sensitivity against changes of the trafficking of newly synthesized vRNA from the RO to the site of translation. For CVB3, our model suggests intra-compartment trafficking two orders of magnitude slower as compared to HCV and DENV, with a highly significant sensitivity of this parameter against changes. A possible explanation may lie in the involvement of different compartments or cell organelles in vRNA translation and replication. All viruses need close proximity to the rough endoplasmic reticulum and its ribosomes for successful vRNA translation; however, they use different cytoplasmic membranes and thus different sites for the formation of their ROs and thus for vRNA synthesis. *Flaviviridae* remodel mainly the rough endoplasmic reticulum, using membrane vesicles or invagination as the site for vRNA translation and synthesis without being exposed to the (possibly damaging) cytoplasmic environment. Melia et al (2019) found that CVB3 uses the rough endoplasmic reticulum first and the Golgi later in infection, suggesting a high degree of flexibility and adaptation of CVB3 to its environment. To what extent viral replication occurs on either membrane is unknown, however, other studies suggest that Golgi-derived membranes serve as the main origin of viral replication [94,99,100]. During CVB3 infection, the Golgi collapsed and was not detectable anymore, suggesting that ROs were Golgi derived [101]. Regarding efficient viral protein production for virion packaging, CVB3 is not enveloped and may only need a fraction of the structural proteins that DENV and HCV needs for assembly (see S1 Supporting text for details), implying that CVB3 developed strategies to overcome longer trafficking distances. However, another explanation may be a possible regulation and competition of vRNA translation and virion packaging. Early in infection, vRNA may be used for translation, while later in infection vRNA may be packaged into virions and thus not available for vRNA translation.

Hypothetical mechanisms behind acute and chronic infections

The plus-strand RNA viruses studied here share the major steps in their life cycle and their replication strategy, but despite these similarities show very different clinical manifestations. While HCV has a relatively mild symptomatic phase, it can establish a chronic infection with low-level viral replication

749 over decades, that goes mostly undetected by the host's immune response. In contrast, DENV causes a
750 vigorous acute self-limited infection that can become life-threatening. Similarly, CVB3 usually causes an
751 acute infection with flu-like symptoms but can become chronic. The underlying mechanisms for the
752 development of chronic infections are unclear, our plus-strand RNA virus replication model might help
753 to reveal the differences in the viral dynamics leading to different clinical manifestations.
754
755 DENV/ZIKV and CVB3 produce a higher ratio of plus- to minus-strand RNA (20:1) compared to HCV, with
756 a plus- to minus-strand RNA ratio of 3:1 (measured in our data) up to 10:1 (reported in literature [102–
757 109]), which may be HCV-strain or cell line-specific. One may speculate that a higher viral RNA synthesis
758 rate may be responsible for the higher plus- to minus-strand RNA ratio in viruses causing acute
759 infections. However, our calculated vRNA synthesis rates were comparable for HCV and DENV, but 50
760 times lower compared to the CVB3 RNA synthesis rate which may be due to faster vRNA copying or
761 faster *de novo* initiation of vRNA synthesis. In HCV, studies found an RNA synthesis rate of 150 to 180
762 nt/min [110,111], however, the rate of RNA synthesis in DENV is to our knowledge unknown.
763 Nevertheless, Tan et al. (1996) found low in vitro polymerase activity for DENV NS5, which is in line with
764 the polymerase activities for West Nile and Kunjin viruses, suggesting that this is a conserved feature of
765 flavivirus polymerases [112] and possibly *Flaviviridae* including HCV.
766
767 As for CVB3, it has been shown that the closely related PV synthesizes a single RNA template in 45 to
768 100 sec [66]. Additionally, it is estimated that between 3 and 10 RdRps are bound to one single PV RNA
769 genome. However, in our plus-strand RNA model, we did not consider the RdRp density bound to one
770 single viral RNA template, due to a lack of data for HCV and DENV. According to our model predictions,
771 key processes for a faster viral life cycle may be a combination of: (1) faster viral RNA translation and
772 synthesis rates and/or faster vRNA synthesis initiation, (2) host cell translation shut-off and thus higher
773 ribosome availability for viral RNA translation and at the same time lower ribosome availability for
774 antiviral protein production, (3) and shorter RNA half-lives for intracellular viral RNA (more important in
775 cell lines with intrinsic immune responses or *in vivo*). Interestingly, the potential role of these key
776 processes is in line with the results of the global sensitivity analysis: All CVB3 replication process rates
777 within the RO show highly significant sensitivities, suggesting that CVB3 strongly depends on an efficient
778 replicative cycle within the RO. Additionally, global sensitivities of vRNA degradation rates in the
779 cytoplasm or within the RO seem rather negligible.
780

Our model predicted that an optimal usage of viral resources to form replicase complexes within a cell was only realized by DENV and CVB3. Strikingly, HCV only reached 26% of the cell's replicase complex carrying capacity. A possible reason may be a limitation in viral resources to form replicase complexes such as viral RNA or non-structural proteins. Both may be again related to the lower availability of ribosomes for viral protein production in HCV, whereas DENV and CVB3 have the advantage of a partial or complete host cell translation shut off, respectively. However, virus-specific differences in the ribosome availability and translation activity may be related to different translation mechanisms. While HCV and CVB3 have IRESes, i.e., the RNA translation is cap-independent, DENV's translation mechanism is cap-dependent. Furthermore, different IRES types have variations in their structural elements and recruit host factors as regulatory elements, which affects the translation initiation complex and viral RNA translation. Therefore, a higher ribosome availability for vRNA translation may be associated with different translation mechanisms such as different secondary structures and host factors assisting in ribosome binding [113–116]. Furthermore, a higher number of ribosomes available for vRNA translation may be directly associated with a higher production of viral proteins. However, the more ribosomes available for cellular mRNA translation and thus the production of proteins of the immune response, the higher may be the intracellular degradation of viral components, resulting in a limitation in viral resources. Ribosome availability and its control may thus be a crucial factor for viral replication efficiency.

To analyze this aspect further, we asked whether we could make virus production in HCV more efficient or CVB3 less efficient. Increasing the *in-silico* ribosome availability in HCV to that of CVB3 increased the viral load by three orders of magnitude. In contrast, a 50-fold increase in the HCV RNA synthesis rate had no effect on the viral load in steady state due to a limited availability of the viral RNA polymerase in the replication organelle [19]. In contrast, using only 0.07% of ribosomes for CVB3 RNA translation, thus setting the ribosome level to the number of ribosomes used in HCV, decreased the CVB3 viral load by three orders of magnitude. Interestingly, the coronaviruses nonstructural proteins, including those of SARS-CoV-2, target multiple processes in the cellular mRNA translation, causing a host cell translation shut off similar to CVB3 and DENV [117,118]. Therefore, a repression or complete shut-off of the host mRNA translation machinery may be a key-feature of acute viral infections.

Comparing *in vivo* viral dynamics with those of *in vitro* experiments is challenging. Nevertheless, we found comparable pattern of viral dynamics: reported *in vivo* and our *in vitro* experiments. *In vivo*, HCV

showed an exponential growth rate of 2.2 per day [119], while DENV and CVB3 grow twice as fast with a rate of 4.3 and 4.5 per day in human and murine blood, respectively (approximated from [38,44]). However, in murine cardiac tissue, the *in vivo* CVB3 exponential growth rate increases to approximately 14.5 per day [38]. Furthermore, the different exponential growth rates are associated with variations in the peak viral load. At its peak, HCV produces 10^8 RNA copies per g liver tissue [43], DENV produces 1 to 2 orders of magnitude more virus (10^9 to 10^{10} RNA copies per ml blood) [44], and CVB3 produces 3 to 4 orders of magnitude more virus (10^{11} to 10^{12} RNA copies per g cardiac tissue) compared to HCV [38]. We found a similar pattern in our data with HCV producing the least amount of virus at its peak (~1 PFU/mL/cell), followed by DENV (~10 PFU/mL/cell) and CVB3 (~200 PFU/mL/cell). Considering the RNA synthesis rates, CVB3 is replicating 50-times faster compared to HCV and DENV.

Broad-spectrum antivirals?

DAAs are highly specific drugs usually designed to inhibit the function of one specific viral protein. Developing broad-spectrum antiviral drugs is challenging. Nevertheless, we were interested in the possibility of a pan-viral drug treatment option. We therefore studied the core processes in the life cycles of our three representatives of plus-strand RNA viruses and administered *in-silico* drugs in mono or combination therapy, with the aim to identify single drug targets or combinations of drug targets that yield an efficient inhibition of all three viruses.

Direct acting antivirals against HCV: Several DAAs have been developed and approved for HCV and are able to cure chronic hepatitis C in the majority of patients [120]. DAAs are developed to target one specific protein such as HCV NS3/4A (e.g., first-generation telaprevir or boceprevir and second-/third generation glecaprevir, voxilaprevir and grazoprevir), HCV NS5A (e.g., daclatasvir, velpatasvir, ledipasvir), and HCV NS5B (e.g., sofosbuvir and dasabuvir) [121]. Therefore, the DAAs' modes of action and efficacies may be used here to validate the results of our *in-silico* drug intervention study. While DAAs blocking HCV NS3/4A intervene with the polyprotein cleavage, HCV NS5A and HCV NS5B inhibitors target the RO formation and vRNA synthesis, respectively [9,59,122]. Our sensitivity and *in-silico* drug analysis suggested high sensitivities for processes associated with HCV RNA replication, which led to an efficient viral reduction by more than 99% with a more than 90% inhibition of the vRNA synthesis rate. Furthermore, our *in-silico* drug analysis predicted that complete HCV NS3/4A inhibition (more than 99.5% polyprotein cleavage inhibition) was necessary to clear the viral load, while in combination with

844 inhibiting vRNA synthesis a combinatory inhibition of more than 90% led to HCV clearance, where viral
845 clearance was mainly driven by inhibiting vRNA synthesis. Our results are in line with current HCV
846 treatment recommendations focusing mainly on a regimen based on a combination of targeting vRNA
847 synthesis alone by inhibiting HCV NS5A and/or NS5B or in combination with HCV NS3/4A, e.g., the
848 combinations of elbasvir (NS5A inhibitor) and grazoprevir (NS3/4A inhibitor), glecaprevir (NS3/4A
849 inhibitor) and pibrentasvir (NS5A inhibitor) or sofosbuvir (NS5B inhibitor) plus velpatasvir (NS5A
850 inhibitor) with the inhibition of NS5A as the backbone of an efficient HCV treatment regimen [123].
851 Interestingly, the combinatory inhibition of vRNA synthesis and polyprotein cleavage showed pan-viral
852 clearance with the lowest critical efficacies of 0.98, i.e., a 98% inhibition of both processes.
853
854 ***Broad-spectrum antivirals and host-directed therapy:*** The cure of a chronic hepatitis C infection
855 represents a success story for DAAs. However, a subset of HCV patients report treatment failure, severe
856 side effects that impede treatment success, or drug resistance [124]. Targeting cellular components that
857 are crucial for successful and efficient viral replication (so-called host dependency factors) may offer a
858 potential treatment option with a high barrier of resistance. Additionally, plus-strand RNA viruses still
859 represent a major health concern infecting millions of people worldwide, including the viruses in this
860 current study – HCV, DENV and CVB3 – and other plus-strand RNA viruses such as chikungunya, Zika,
861 West Nile, Yellow fever, hepatitis A virus as well as the current global pandemic causing SARS-CoV-2.
862 Even though the identification of pan-serotype antiviral agents is challenging, a DENV inhibitor has been
863 identified, which has shown high efficacy and pan-serotype activity against all known DENV genotypes
864 and serotypes [125]. Our model may serve as a basis towards the development of further virus-specific
865 models as well as pan-viral broad-spectrum antiviral treatment strategies.
866
867 Our sensitivity and drug analysis showed that inhibiting translation complex formation, vRNA translation
868 or polyprotein cleavage in combination with vRNA synthesis represent the most promising pan-viral
869 drug targets. As in the case of HCV, targeting vRNA replication and polyprotein cleavage has been highly
870 successful, however, directly targeting the HCV RNA translation (e.g., the HCV IRES RNA structure) or its
871 complex formation is mainly experimental. Another treatment strategy may be targeting host factors
872 hijacked by the virus and involved in almost every process of the viral life cycle [126]. We found that a
873 limitation in the number of available ribosomes may be a key feature limiting efficient virus production
874 due to suppressed host mRNA translation or complete host cell translation shut-off. However, targeting
875 and thus inhibiting the biological function of ribosomes will obviously be challenging and not beneficial

for the host. Nevertheless, two proteins were found interacting with vRNA translation: RACK1 and RPS25. Both proteins may be hijacked by DENV and promote DENV mediated cap-independent RNA translation [127]. Additionally, in HCV RACK1 has been shown to inhibit IRES mediated viral RNA translation and viral replication; in the latter case RACK1 binds to HCV NS5A, which induces the formation of ROs [128,129]. Similar to HCV, CVB3 RNA translation is mediated through an IRES and thus RACK1 may be a potential drug target. Furthermore, studying interactions of SARS-CoV-2 proteins with host mRNA identified RACK1 as a binding partner and thus may represent a pan-viral host dependency factor [130].

Interestingly, the very early processes in the viral life cycle, virus entry as well as fusion and release of the vRNA genome, showed significant sensitivities in DENV and CVB3 but was rather negligible in HCV. Further, the release of the viral RNA genome from endosomes showed a higher significant sensitivity compared to viral entry and internalization. Interestingly, cyclophilin A seems to be a host factor involved in the enterovirus A71 (family *Picornaviridae*) fusion/uncoating process and thus vRNA release [131,132]. Furthermore, cyclophilin A inhibitors successfully block or decrease viral replication in a number of plus-strand RNA viruses such as HCV, DENV, West-Nile virus, yellow fever virus, enteroviral A71 and coronavirus [133,134]. Considering that it is involved in both processes that showed highest sensitivities, cyclophilin A may represent a promising pan-viral target [134].

The formation of the replicase complexes represented another sensitive pan-viral process. Replicase complexes are associated with membranes of the ROs either within or outside the RO facing the cytosol [135]. Several studies have shown the significance of host factors in the RO formation being associated with cell permissiveness and vRNA replication efficiency [17,89,118,126]. For example, Tabata et al. (2021) have shown that the RO biogenesis in HCV and SARS-CoV-2 critically depends on the lipid phosphatidic acid synthesis, since inhibiting associated pathways led to an impaired HCV and SARS-CoV-2 RNA replication [136]. However, even though successful in clearing HCV and DENV, in an established infection of a fast-replicating virus such as CVB3, the formation of replicase complexes may not represent an efficient drug target. In steady state, CVB3 replicase complexes are already formed, and the virus cannot be cleared even with a 100% inhibition given for 5 days. Similar results have been found by targeting host factors involved in the formation of replicase complexes of other picornaviruses. Two tested compounds targeting RO formation were not able to block viral replication suggesting that if ROs are already formed, the viral replication continues [137]. Furthermore, targeting host factors involved in

RO formation showed lethal cytotoxicity as in the case of PI4KIIIβ and HCV [138]. Interestingly, inhibiting the host factor PI4KB showed that CVB3 RO formation was delayed and CVB3 RNA replication occurred at the Golgi apparatus [139].

Interestingly, incomplete inhibition of some processes may promote viral growth. Our model predicted that targeting viral export from the RO into the cytoplasm in the DENV life cycle led to a 6% increase in virus. Therefore, low-efficacy drugs may lead to the opposite of the desired outcome. Thus, host directed therapy may have a huge potential on the one hand but may result in substantial side effects on the other hand. The identification of host factors with pan-viral activity without lethal toxicity represents a challenge for future research.

Limitations and outlook

In the current study, we developed the first mathematical model for the intracellular replication of a group of related plus-strand RNA viruses. Even though our model allowed a high degree of parameter identifiability, fit the *in vitro* kinetic data, and is consistent with the current biological knowledge of our studied viruses, there are some weaknesses to consider.

First, our model focuses on a single cell, and hence does not include viral spread. Especially in acute infections with rapidly replicating viruses, viral transmission within organs may be highly relevant to consider. However, since our model was developed for a single step growth curve, we neglected viral spread and focused mainly on intracellular replication processes. Virus-specific mechanisms of viral spread from infected to susceptible cells may be interesting to study in the future.

Second, our experiments were performed in the immuno-compromised Huh7 cell line, we did not consider an intrinsic immune response here. In the future, considering an intrinsic immune response may be an important addition.

Third, even though plus-strand RNA viruses share remarkable similarities in their replication strategy, our model does not consider viruses with more than one open reading frame and ribosomal frameshift. The difference between viruses with one and more open reading frames is the presence of sub-genomic RNA, as in the case of coronaviruses. However, the life cycle of coronaviruses, and in particular SARS-

CoV-2, differs from our model by producing non-structural proteins first, followed by viral RNA and sub-genomic RNA synthesis [140]. The sub-genomic RNA is later translated into structural proteins. However, since the core processes of viral non-structural protein production (necessary for vRNA synthesis) and vRNA synthesis itself are common, we do not think that the presence of sub-genomic RNA would have a huge impact on our presented results. Adaptation of the model to coronaviruses is an ongoing topic being followed up in our group.

Fourth, *in vitro* experiments are not a reliable system for an *in vivo* application. Especially our drug treatment study needs experimental validation. However, our model and *in silico* drug analysis showed a high degree of similarity with knowledge and efficacy of DAAs available for HCV.

Fifth, our model has been developed for a one step growth experiment and consequently a single cycle of virus growth. Thus, our model predictions are of a short-term nature and do not study long-term effects.

In summary, in the present study we measured the *in vitro* kinetics of three representatives of plus-strand RNA viruses: HCV, DENV, and CVB3. Based on these experimental measurements, we developed a mathematical model of the intracellular plus-strand RNA virus life cycle. In order to study pan-viral similarities and virus-specific differences, the model was fit simultaneously to the *in vitro* measurements, where the best-fit model was selected based on the AIC and model parameter identifiability. According to our model, the viral life cycles of our three plus-strand RNA representatives differ mainly in processes of viral entry and genome release, the availability of ribosomes involved in viral RNA translation, formation of the replicase complex, and viral trafficking of newly produced viral RNA. Furthermore, our model predicted that the availability of ribosomes involved in viral RNA translation and thus the degree of the host cell translation shut-off may play a key role in acute infection outcome. Interestingly, our modelling predicted that increasing the number of ribosomes available for HCV RNA translation remarkably enhanced the HCV RNA replication efficiency and increased the HCV viral load by three orders of magnitude, a feature we were not able to achieve by increasing the HCV RNA synthesis rate. Furthermore, according to our *in-silico* drug analysis, we found that targeting processes associated with vRNA translation especially polyprotein cleavage together with viral RNA replication substantially decreased viral load and may represent promising drug targets with broad-spectrum antiviral activity.

971

972 Abbreviations

973

974	CVB3	Coxsackievirus B3
975	DAA	Direct acting antivirals
976	DENV	Dengue virus
977	d pi	days post infection
978	HCV	Hepatitis C virus
979	h pi	hours post infection
980	ODE	Ordinary differential equations
981	PV	Poliovirus
982	RdRp	RNA-dependent RNA polymerase
983	RO	Replication organelle
984	ZIKV	Zika virus

985

986 References

987

988 1. Ciotti M, Angeletti S, Minieri M, Giovannetti M, Benvenuto D, Pascarella S, et al. COVID-19
989 outbreak: An overview. Chemotherapy. 2020;64: 215–223. doi:10.1159/000507423

990 2. World Health Organization. WHO coronavirus (COVID-19) dashboard with vaccination data. In:
991 WHO [Internet]. 2021 [cited 7 Mar 2022] pp. 1–5. Available: https://covid19.who.int/

992 3. Cutler DM, Summers LH. The COVID-19 pandemic and the $16 trillion virus. JAMA - Journal of the
993 American Medical Association. American Medical Association; 2020. pp. 1495–1496.
994 doi:10.1001/jama.2020.19759

995 4. Shepard DS, Undurraga EA, Halasa YA, Stanaway JD. The global economic burden of dengue: a
996 systematic analysis. Lancet Infect Dis. 2016;16: 935–941. doi:10.1016/S1473-3099(16)00146-8

997 5. United Nations. A socio-economic impact assessment of the Zika virus in Latin America and the
998 Caribbean. 2017. Available: http://www.undp.org/content/undp/en/home/librarypage/hiv-
999 aids/a-socio-economic-impact-assessment-of-the-zika-virus-in-latin-am.html

6. Barber MJ, Gotham D, Khwairakpam G, Hill A. Price of a hepatitis C cure: Cost of production and current prices for direct-acting antivirals in 50 countries. J Virus Erad. 2020;6: 100001. doi:10.1016/J.JVE.2020.06.001

7. Shakeri A, Srimurugathasan N, Suda KJ, Gomes T, Tadrous M. Spending on Hepatitis C Antivirals in the United States and Canada, 2014 to 2018. Value Heal. 2020;23: 1137–1141. doi:10.1016/J.JVAL.2020.03.021

8. FDA. Coronavirus (COVID-19) update: FDA authorizes first oral antiviral for treatment of COVID-19. In: Food and Drug Administration [Internet]. 2021 p. 1. Available: https://www.fda.gov/news-events/press-announcements/coronavirus-covid-19-update-fda-authorizes-first-oral-antiviral-treatment-covid-19

9. Hayes CN, Imamura M, Tanaka J, Chayama K. Road to elimination of HCV: Clinical challenges in HCV management. Liver International. John Wiley & Sons, Ltd; 2022. doi:10.1111/liv.15150

10. World Health Organization. Hepatitis C. 2019. Available: https://www.who.int/news-room/fact-sheets/detail/hepatitis-c

11. World Health Organization. Dengue and severe dengue. 2016. doi:10.1111/1469-0691.12442

12. Colpitts CC, El-Saghire H, Pochet N, Schuster C, Baumert TF. High-throughput approaches to unravel hepatitis C virus-host interactions. Virus Res. 2016;218: 18–24. doi:10.1016/j.virusres.2015.09.013

13. Genoni A, Canducci F, Rossi A, Broccolo F, Chumakov K, Bono G, et al. Revealing enterovirus infection in chronic human disorders: An integrated diagnostic approach. Sci Rep. 2017;7: 5013. doi:10.1038/s41598-017-04993-y

14. Baggen J, Thibaut HJ, Strating JRPM, Van Kuppeveld FJM. The life cycle of non-polio enteroviruses and how to target it. Nature Reviews Microbiology. Nat Rev Microbiol; 2018. pp. 368–381. doi:10.1038/s41579-018-0005-4

15. Garmaroudi FS, Marchant D, Hendry R, Luo H, Yang D, Ye X, et al. Coxsackievirus B3 replication and pathogenesis. 2015;10: 629–652.

16. Romero-Brey I, Merz A, Chiramel A, Lee JY, Chlanda P, Haselman U, et al. Three-dimensional architecture and biogenesis of membrane structures associated with hepatitis C virus replication.

Luo GG, editor. PLoS Pathog. 2012;8: e1003056. doi:10.1371/journal.ppat.1003056

17. Belov GA, van Kuppeveld FJ. (+)RNA viruses rewire cellular pathways to build replication organelles. Curr Opin Virol. 2012;2: 740–747. doi:10.1016/j.coviro.2012.09.006

18. Miller S, Krijnse-Locker J. Modification of intracellular membrane structures for virus replication. Nat Rev Microbiol. 2008;6: 363–374. doi:10.1038/nrmicro1890

19. Binder M, Sulaimanov N, Clausznitzer D, Schulze M, Hüber CM, Lenz SM, et al. Replication vesicles are load- and choke-points in the hepatitis C virus lifecycle. PLoS Pathog. 2013;9: e1003561. doi:10.1371/journal.ppat.1003561

20. Paul D, Bartenschlager R. Architecture and biogenesis of plus-strand RNA virus replication factories. World J Virol. 2013;2: 32–48. doi:10.5501/wjv.v2.i2.32

21. Limpens RWAL, van der Schaar HM, Kumar D, Koster AJ, Snijder EJ, van Kuppeveld FJM, et al. The transformation of enterovirus replication structures: A three-dimensional study of single- and double-membrane compartments. MBio. 2011;2. doi:10.1128/mBio.00166-11

22. Gale M, Tan SL, Katze MG. Translational control of viral gene expression in eukaryotes. Microbiol Mol Biol Rev. 2000;64: 239–80. doi:10.1128/MMBR.64.2.239-280.2000

23. Roth H, Magg V, Uch F, Mutz P, Klein P, Haneke K, et al. Flavivirus infection uncouples translation suppression from cellular stress responses. MBio. 2017;8. doi:10.1128/mBio.02150-16

24. Huang J-Y, Su W-C, Jeng K-S, Chang T-H, Lai MMC. Attenuation of 40S ribosomal subunit abundance differentially affects host and HCV translation and suppresses HCV replication. PLoS Pathog. 2012;8: e1002766. doi:10.1371/journal.ppat.1002766

25. Zitzmann C, Kaderali L. Mathematical analysis of viral replication dynamics and antiviral treatment strategies: From basic models to age-based multi-scale modeling. Front Microbiol. Frontiers; 2018. p. 1546. doi:10.3389/fmicb.2018.01546

26. Perelson AS, Ke R. Mechanistic modelling of SARS-CoV-2 and other infectious diseases and the effects of therapeutics. Clin Pharmacol Ther. 2021. doi:10.1002/cpt.2160

27. Layden TJ, Layden JE, Ribeiro RM, Perelson AS. Mathematical modeling of viral kinetics: A tool to understand and optimize therapy. Clin Liver Dis. 2003;7: 163–178. doi:10.1016/S1089-3261(02)00063-6

28. Perelson AS, Ribeiro RM. Hepatitis B virus kinetics and mathematical modeling. Semin Liver Dis. 2004;24: 11–16. doi:10.1055/s-2004-828673

29. Smith AM, Perelson AS. Influenza A virus infection kinetics: Quantitative data and models. Wiley Interdiscip Rev Syst Biol Med. 2011;3: 429–445. doi:10.1002/wsbm.129

30. Bonhoeffer S, Coffin JM, Nowak MA. Human Immunodeficiency Virus Drug Therapy and Virus Load. J Virol. 1997;71: 3275–3278.

31. Perelson AS, Ribeiro RM. Modeling the within-host dynamics of HIV infection. BMC Biol. 2013;11: 96. doi:10.1186/1741-7007-11-96

32. Tuiskunen Bäck A, Lundkvist Å. Dengue viruses – an overview. Infect Ecol Epidemiol. 2013;3: 19839. doi:10.3402/iee.v3i0.19839

33. Moradpour D, Penin F, Rice CM. Replication of hepatitis C virus. J Gen Virol. 2007;5: 453–463. doi:10.1038/nrmicro1645

34. Chen BS, Lee HC, Lee KM, Gong YN, Shih SR. Enterovirus and encephalitis. Frontiers in Microbiology. Frontiers Media S.A.; 2020. p. 261. doi:10.3389/fmicb.2020.00261

35. Koestner W, Spanier J, Klause T, Tegtmeyer P-K, Becker J, Herder V, et al. Interferon-beta expression and type I interferon receptor signaling of hepatocytes prevent hepatic necrosis and virus dissemination in Coxsackievirus B3-infected mice. Lemon SM, editor. PLOS Pathog. 2018;14: e1007235. doi:10.1371/journal.ppat.1007235

36. WHO. Hepatitis C. 2019 [cited 20 Aug 2019]. Available: https://www.who.int/news-room/fact-sheets/detail/hepatitis-c

37. J. E Cogan. Dengue and severe dengue. In: World Health Organization [Internet]. 2018. Available: https://www.who.int/news-room/fact-sheets/detail/dengue-and-severe-dengue

38. Reetoo KN, Osman SA, Illavia SJ, Cameron-Wilson CL, Banatvala JE, Muir P. Quantitative analysis of viral RNA kinetics in coxsackievirus B3-induced murine myocarditis: Biphasic pattern of clearance following acute infection, with persistence of residual viral RNA throughout and beyond the inflammatory phase of disease. J Gen Virol. 2000;81: 2755–2762. doi:10.1099/0022-1317-81-11-2755

39. Pybus OG, Charleston MA, Gupta S, Rambaut A, Holmes EC, Harvey PH. The epidemic behavior of

1084 the hepatitis C virus. Science (80-). 2001;292: 2323–2325. doi:10.1126/science.1058321

1085 40. Liu Y, Lillepold K, Semenza JC, Tozan Y, Quam MBM, Rocklöv J. Reviewing estimates of the basic
1086 reproduction number for dengue, Zika and chikungunya across global climate zones.
1087 Environmental Research. Academic Press Inc.; 2020. p. 109114.
1088 doi:10.1016/j.envres.2020.109114

1089 41. Lim CTK, Jiang L, Ma S, James L, Ang LW. Basic reproduction number of coxsackievirus type A6
1090 and A16 and enterovirus 71: Estimates from outbreaks of hand, foot and mouth disease in
1091 Singapore, a tropical city-state. Epidemiol Infect. 2016;144: 1028–1034.
1092 doi:10.1017/S0950268815002137

1093 42. Ma E, Fung C, Yip SHL, Wong C, Chuang SK, Tsang T. Estimation of the basic reproduction number
1094 of enterovirus 71 and coxsackievirus A16 in hand, foot, and mouth disease outbreaks. Pediatr
1095 Infect Dis J. 2011;30: 675–679. doi:10.1097/INF.0b013e3182116e95

1096 43. Martinelli A de LC, Brown D, Morris A, Dhillon A, Dayley P, Dusheiko G. Quantitation of HCV RNA
1097 in liver of patients with chronic hepatitis C. Arq Gastroenterol. 2000;37: 203–207.
1098 doi:10.1590/S0004-28032000000400003

1099 44. Ben-Shachar R, Koelle K. Transmission-clearance trade-offs indicate that dengue virulence
1100 evolution depends on epidemiological context. Nat Commun. 2018;9: 2355. doi:10.1038/s41467-
1101 018-04595-w

1102 45. Major ME, Dahari H, Mihalik K, Puig M, Rice CM, Neumann AU, et al. Hepatitis C virus kinetics and
1103 host responses associated with disease and outcome of infection in chimpanzees. Hepatology.
1104 2004;39: 1709–1720. doi:10.1002/hep.20239

1105 46. Nainan O V., Alter MJ, Kruszon-Moran D, Gao FX, Xia G, McQuillan G, et al. Hepatitis C virus
1106 genotypes and viral concentrations in participants of a general population survey in the United
1107 States. Gastroenterology. 2006;131: 478–484. doi:10.1053/j.gastro.2006.06.007

1108 47. Hajarizadeh B, Grady B, Page K, Kim AY, McGovern BH, Cox AL, et al. Patterns of hepatitis C Virus
1109 RNA levels during acute infection: The InC3 study. Blackard J, editor. PLoS One. 2015;10:
1110 e0122232. doi:10.1371/journal.pone.0122232

1111 48. Cherry JD, Krogstad P. Enterovirus and parechovirus infections. Infectious Diseases of the Fetus

and Newborn Infant. W.B. Saunders; 2011. pp. 756–799. doi:10.1016/B978-1-4160-6400-8.00024-9

49. Koutsoudakis G, Herrmann E, Kallis S, Bartenschlager R, Pietschmann T. The level of CD81 cell surface expression is a key determinant for productive entry of hepatitis C virus into host cells. J Virol. 2007;81: 588–598. doi:10.1128/jvi.01534-06

50. Dächert C, Gladilin E, Binder M. Gene expression profiling of different HuH7 variants reveals novel hepatitis C virus host factors. Viruses. 2019;12. doi:10.3390/v12010036

51. P C, N S. Single-step method of RNA isolation by acid guanidinium thiocyanate-phenol-chloroform extraction. Anal Biochem. 1987;162: 156–159. doi:10.1006/ABIO.1987.9999

52. Grünvogel O, Colasanti O, Lee JY, Klöss V, Belouzard S, Reustle A, et al. Secretion of hepatitis C virus replication intermediates reduces activation of toll-like receptor 3 in hepatocytes. Gastroenterology. 2018;154: 2237-2251.e16. doi:10.1053/j.gastro.2018.03.020

53. Lanke KHW, van der Schaar HM, Belov GA, Feng Q, Duijsings D, Jackson CL, et al. GBF1, a guanine nucleotide exchange factor for Arf, is crucial for coxsackievirus B3 RNA replication. J Virol. 2009;83: 11940–9. doi:10.1128/JVI.01244-09

54. Feng Q, Hato S V., Langereis MA, Zoll J, Virgen-Slane R, Peisley A, et al. MDA5 detects the double-stranded RNA replicative form in picornavirus-infected cells. Cell Rep. 2012;2: 1187–1196. doi:10.1016/j.celrep.2012.10.005

55. Zitzmann C, Schmid B, Ruggieri A, Perelson AS, Binder M, Bartenschlager R, et al. A coupled mathematical model of the intracellular replication of dengue virus and the host cell immune response to infection. Front Microbiol. 2020;11: 725. doi:10.3389/fmicb.2020.00725

56. Schmid B, Rinas M, Ruggieri A, Acosta EG, Bartenschlager M, Reuter A, et al. Live cell analysis and mathematical modeling identify determinants of attenuation of dengue virus 2-O-methylation mutant. PLoS Pathog. 2015;11: e1005345. doi:10.1371/journal.ppat.1005345

57. Zitzmann C, Kaderali L, Perelson AS. Mathematical modeling of hepatitis C RNA replication, exosome secretion and virus release. PLoS Comput Biol. 2020;16: e1008421. doi:10.1371/journal.pcbi.1008421

58. Kazakov T, Yang F, Ramanathan HN, Kohlway A, Diamond MS, Lindenbach BD. Hepatitis C virus

RNA replication depends on specific cis- and trans-acting activities of viral nonstructural proteins. PLoS Pathog. 2015;11: e1004817. doi:10.1371/journal.ppat.1004817

59. Benzine T, Brandt R, Lovell WC, Yamane D, Neddermann P, De Francesco R, et al. NS5A inhibitors unmask differences in functional replicase complex half-life between different hepatitis C virus strains. Randall G, editor. PLOS Pathog. 2017;13: e1006343. doi:10.1371/journal.ppat.1006343

60. Heldt FS, Frensing T, Reichl U. Modeling the intracellular dynamics of influenza virus replication to understand the control of viral RNA synthesis. J Virol. 2012;86: 7806–17. doi:10.1128/JVI.00080-12

61. Laske T, Heldt FS, Hoffmann H, Frensing T, Reichl U. Modeling the intracellular replication of influenza A virus in the presence of defective interfering RNAs. Virus Res. 2016;213: 90–99. doi:10.1016/j.virusres.2015.11.016

62. Raue A, Steiert B, Schelker M, Kreutz C, Maiwald T, Hass H, et al. Data2Dynamics: a modeling environment tailored to parameter estimation in dynamical systems. Bioinformatics. 2015;31: 3558–3560. doi:10.1093/bioinformatics/btv405

63. Raue A, Kreutz C, Maiwald T, Bachmann J, Schilling M, Klingmüller U, et al. Structural and practical identifiability analysis of partially observed dynamical models by exploiting the profile likelihood. Bioinformatics. 2009;25: 1923–1929. doi:10.1093/bioinformatics/btp358

64. Marino S, Hogue IB, Ray CJ, Kirschner DE. A methodology for performing global uncertainty and sensitivity analysis in systems biology. J Theor Biol. 2008;254: 178–96. doi:10.1016/j.jtbi.2008.04.011

65. Aunins TR, Marsh KA, Subramanya G, Uprichard SL, Perelson AS, Chatterjee A. Intracellular hepatitis C modeling predicts infection dynamics and viral protein mechanisms. J Virol. 2018;92: JVI.02098-17. doi:10.1128/JVI.02098-17

66. Regoes RR, Crotty S, Antia R, Tanaka MM. Optimal replication of poliovirus within cells. Am Nat. 2005;165: 364–73. doi:10.1086/428295

67. Byk LA, Iglesias NG, De Maio FA, Gebhard LG, Rossi M, Gamarnik A V. Dengue virus genome uncoating requires ubiquitination. MBio. 2016;7: e00804-16. doi:10.1128/mBio.00804-16

68. Simoes EA, Sarnow P. An RNA hairpin at the extreme 5’ end of the poliovirus RNA genome

1168 modulates viral translation in human cells. J Virol. 1991;65: 913–921. doi:10.1128/jvi.65.2.913-
1169 921.1991

1170 69. Gohara DW, Arnold JJ, Cameron CE. Poliovirus RNA-dependent RNA polymerase (3Dpol): Kinetic,
1171 thermodynamic, and structural analysis of ribonucleotide selection. Biochemistry. 2004;43:
1172 5149–5158. doi:10.1021/bi035429s

1173 70. Goo L, Dowd KA, Smith ARY, Pelc RS, Demaso CR, Pierson TC. Zika virus is not uniquely stable at
1174 physiological temperatures compared to other flaviviruses. MBio. 2016;7.
1175 doi:10.1128/mBio.01396-16

1176 71. Carson SD, Hafenstein S, Lee H. MOPS and coxsackievirus B3 stability. Virology. 2017;501: 183–
1177 187. doi:10.1016/j.virol.2016.12.002

1178 72. Carson SD, Chapman NM, Hafenstein S, Tracy S. Variations of coxsackievirus B3 capsid primary
1179 structure, ligands, and stability Are selected for in a coxsackievirus and adenovirus receptor-
1180 limited environment. J Virol. 2011;85: 3306–3314. doi:10.1128/jvi.01827-10

1181 73. Persaud M, Martinez-Lopez A, Buffone C, Porcelli SA, Diaz-Griffero F. Infection by Zika viruses
1182 requires the transmembrane protein AXL, endocytosis and low pH. Virology. 2018;518: 301–312.
1183 doi:10.1016/j.virol.2018.03.009

1184 74. Chatel-Chaix L, Bartenschlager R. Dengue virus- and hepatitis C virus-induced replication. J Virol.
1185 2014;88: 5907–5911.

1186 75. Perelson AS, Neumann AU, Markowitz M, Leonard JM, Ho DD. HIV-1 dynamics in vivo: virion
1187 clearance rate, infected cell life-span, and viral generation time. Science (80-). 1996;271: 1582–
1188 1586. doi:10.1126/science.271.5255.1582

1189 76. Neumann AU, Lam NP, Dahari H, Gretch DR, Wiley TE, Layden TJ, et al. Hepatitis C viral dynamics
1190 in vivo and the antiviral efficacy of interferon-α therapy. Science (80-). 1998;282: 103–107.
1191 doi:10.1126/science.282.5386.103

1192 77. Perelson AS, Essunger P, Cao Y, Vesanen M, Hurley A, Saksela K, et al. Decay characteristics of
1193 HIV-1-infected compartments during combination therapy. Nature. 1997;387: 188–191.
1194 doi:10.1038/387188a0

1195 78. Baccam P, Beauchemin C, Macken CA, Hayden FG, Perelson AS. Kinetics of influenza A virus

1196 infection in humans. J Virol. 2006;80: 7590–9. doi:10.1128/JVI.01623-05

1197 79. Dahari H, Ribeiro RM, Rice CM, Perelson AS. Mathematical modeling of subgenomic hepatitis C
1198 virus replication in Huh-7 cells. J Virol. 2007;81: 750–60. doi:10.1128/JVI.01304-06

1199 80. Quintela B de M, Conway JM, Hyman JM, Guedj J, dos Santos RW, Lobosco M, et al. A new age-
1200 structured multiscale model of the hepatitis C virus life-cycle during infection and therapy with
1201 direct-acting antiviral agents. Front Microbiol. 2018;9: 601. doi:10.3389/fmicb.2018.00601

1202 81. Reddy B, Yin J. Quantitative intracellular kinetics of HIV type 1. AIDS Res Hum Retroviruses.
1203 1999;15: 273–283. doi:10.1089/088922299311457

1204 82. Heldt FS, Frensing T, Pflugmacher A, Gröpler R, Peschel B, Reichl U. Multiscale modeling of
1205 influenza A virus infection supports the development of direct-acting antivirals. Koelle K, editor.
1206 PLoS Comput Biol. 2013;9: e1003372. doi:10.1371/journal.pcbi.1003372

1207 83. Reichl U, Sidorenko Y. Dynamics of virus-host cell interaction. Bioinformatics-From Genomes to
1208 Therapies. Weinheim, Germany: Wiley-VCH Verlag GmbH; 2008. pp. 861–898.
1209 doi:10.1002/9783527619368.ch23

1210 84. Frensing T, Heldt FS, Pflugmacher A, Behrendt I, Jordan I, Flockerzi D, et al. Continuous influenza
1211 virus production in cell culture shows a periodic accumulation of defective interfering particles.
1212 Pöhlmann S, editor. PLoS One. 2013;8: e72288. doi:10.1371/journal.pone.0072288

1213 85. Heldt FS, Kupke SY, Dorl S, Reichl U, Frensing T. Single-cell analysis and stochastic modelling
1214 unveil large cell-to-cell variability in influenza A virus infection. Nat Commun. 2015;6: 8938.
1215 doi:10.1038/ncomms9938

1216 86. Sidorenko Y, Voigt A, Schulze-Horsel J, Reichl U, Kienle A. Stochastic population balance modeling
1217 of influenza virus replication in vaccine production processes. II. Detailed description of the
1218 replication mechanism. Chem Eng Sci. 2008. doi:10.1016/j.ces.2007.12.034

1219 87. Sidorenko Y, Reichl U. Structured model of influenza virus replication in MDCK cells. Biotechnol
1220 Bioeng. 2004;88: 1–14. doi:10.1002/bit.20096

1221 88. Chhajer H, Rizvi VA, Roy R. Life cycle process dependencies of positive-sense RNA viruses suggest
1222 strategies for inhibiting productive cellular infection. J R Soc Interface. 2021;18.
1223 doi:10.1098/RSIF.2021.0401

89. Baggen J, Thibaut HJ, Strating JRPM, Van Kuppeveld FJM. The life cycle of non-polio enteroviruses and how to target it. Nature Reviews Microbiology. Nature Publishing Group; 2018. pp. 368–381. doi:10.1038/s41579-018-0005-4

90. Lohmann V, Bartenschlager R. On the history of hepatitis C virus cell culture systems. J Med Chem. 2014;57: 1627–1642. doi:10.1021/JM401401N

91. Fischl W, Bartenschlager R. Exploitation of cellular pathways by Dengue virus. Current Opinion in Microbiology. 2011. pp. 470–475. doi:10.1016/j.mib.2011.07.012

92. Clyde K, Kyle JL, Harris E. Recent advances in deciphering viral and host determinants of dengue virus replication and pathogenesis. J Virol. 2006;80: 11418–11431. doi:10.1128/jvi.01257-06

93. Anderson R. Manipulation of cell surface macromolecules by flaviviruses. Adv Virus Res. 2003;59: 229–274. doi:10.1016/S0065-3527(03)59007-8

94. Hsu NY, Ilnytska O, Belov G, Santiana M, Chen YH, Takvorian PM, et al. Viral reorganization of the secretory pathway generates distinct organelles for RNA replication. Cell. 2010;141: 799–811. doi:10.1016/j.cell.2010.03.050

95. Bushell M, Sarnow P. Hijacking the translation apparatus by RNA viruses. Journal of Cell Biology. The Rockefeller University Press; 2002. pp. 395–399. doi:10.1083/jcb.200205044

96. Summers DF, Maizel J V., Darnell JE. The decrease in size and synthetic activity of poliovirus polysomes late in the infectious cycle. Virology. 1967;31: 427–435. doi:10.1016/0042-6822(67)90222-X

97. Boersma S, Rabouw HH, Bruurs LJM, Pavlovič T, van Vliet ALW, Beumer J, et al. Translation and replication dynamics of single RNA viruses. Cell. 2020;183: 1930-1945.e23. doi:10.1016/j.cell.2020.10.019

98. Reid DW, Campos RK, Child JR, Zheng T, Chan KWK, Bradrick SS, et al. Dengue virus selectively annexes endoplasmic reticulum-associated translation machinery as a strategy for co-opting host cell protein synthesis. J Virol. 2018;92: 1766–1783. doi:10.1128/jvi.01766-17

99. Melia CE, Peddie CJ, de Jong AWM, Snijder EJ, Collinson LM, Koster AJ, et al. Origins of enterovirus replication organelles established by whole-cell electron microscopy. MBio. 2019;10. doi:10.1128/mbio.00951-19

100. Melia CE, van der Schaar HM, Lyoo H, Limpens RWAL, Feng Q, Wahedi M, et al. Escaping host factor PI4KB inhibition: Enterovirus genomic RNA replication in the absence of replication organelles. Cell Rep. 2017;21: 587–599. doi:10.1016/j.celrep.2017.09.068

101. Li X, Wang M, Cheng A, Wen X, Ou X, Mao S, et al. Enterovirus replication o organelles and inhibitors of their formation. Frontiers in Microbiology. Frontiers Media S.A.; 2020. p. 1817. doi:10.3389/fmicb.2020.01817

102. Iglesias NG, Gamarnik A V. RNA Biology Dynamic RNA structures in the dengue virus genome. 2011 [cited 6 Aug 2020]. doi:10.4161/rna.8.2.14992

103. Villordo SM, Alvarez DE, Gamarnik A V. A balance between circular and linear forms of the dengue virus genome is crucial for viral replication. RNA. 2010;16: 2325–2335. doi:10.1261/rna.2120410

104. Bolten R, Egger D, Gosert R, Schaub G, Landmann L, Bienz K. Intracellular localization of poliovirus plus- and minus-Strand RNA visualized by strand-specific fluorescent in situ hybridization. J Virol. 1998;72: 8578–8585. doi:10.1128/jvi.72.11.8578-8585.1998

105. Guo J-T, Bichko V V., Seeger C. Effect of alpha interferon on the hepatitis C virus replicon. J Virol. 2001;75: 8516–8523. doi:10.1128/jvi.75.18.8516-8523.2001

106. Quinkert D, Bartenschlager R, Lohmann V. Quantitative analysis of the hepatitis C virus replication complex. J Virol. 2005;79: 13594–13605. doi:10.1128/jvi.79.21.13594-13605.2005

107. Iwasaki A, Medzhitov R. Innate responses to viral infections. 6th ed. In: Fields BN, Knipe DM, Howley PM, editors. Fields Virology: Sixth Edition. 6th ed. Wolters Kluwer Health/Lippincott Williams & Wilkins; 2013. pp. 189–213.

108. Boersma S, Rabouw HH, Bruurs LJM, Pavlovič T, van Vliet ALW, Beumer J, et al. Translation and replication dynamics of single RNA viruses. Cell. 2020;183: 1930-1945.e23. doi:10.1016/j.cell.2020.10.019

109. Lohmann V, Körner F, Koch JO, Herian U, Theilmann L, Bartenschlager R. Replication of subgenomic hepatitis C virus RNAs in a hepatoma cell line. Science (80-). 1999;285: 110–113. doi:10.1126/science.285.5424.110

110. Oh J-W, Ito T, Lai MMC. A recombinant hepatitis C virus RNA-dependent RNA polymerase capable

of copying the full-length viral RNA. J Virol. 1999;73: 7694–7702. doi:10.1128/jvi.73.9.7694-7702.1999

111. Ma H, Leveque V, De Witte A, Li W, Hendricks T, Clausen SM, et al. Inhibition of native hepatitis C virus replicase by nucleotide and non-nucleoside inhibitors. Virology. 2005;332: 8–15. doi:10.1016/j.virol.2004.11.024

112. Tan BH, Fu J, Sugrue RJ, Yap EH, Chan YC, Tan YH. Recombinant dengue type 1 virus NS5 protein expressed in Escherichia coli exhibits RNA-dependent RNA polymerase activity. Virology. 1996;216: 317–325. doi:10.1006/viro.1996.0067

113. Yang Y, Wang Z. IRES-mediated cap-independent translation, a path leading to hidden proteome. J Mol Cell Biol. 2019;11: 911–919. doi:10.1093/JMCB/MJZ091

114. Lee KM, Chen CJ, Shih SR. Regulation mechanisms of viral IRES-driven translation. Trends in Microbiology. Elsevier; 2017. pp. 546–561. doi:10.1016/j.tim.2017.01.010

115. Pelletier J, Sonenberg N. The organizing principles of eukaryotic ribosome recruitment. Annual Review of Biochemistry. 2019. pp. 307–335. doi:10.1146/annurev-biochem-013118-111042

116. Fernández-García L, Angulo J, Ramos H, Barrera A, Pino K, Vera-Otarola J, et al. The internal ribosome entry site of dengue virus mRNA is Active when cap-dependent translation initiation is inhibited. J Virol. 2021;95. doi:10.1128/jvi.01998-20

117. Finkel Y, Gluck A, Nachshon A, Winkler R, Fisher T, Rozman B, et al. SARS-CoV-2 uses a multipronged strategy to impede host protein synthesis. Nature. 2021;594: 240–245. doi:10.1038/s41586-021-03610-3

118. de Wilde AH, Snijder EJ, Kikkert M, van Hemert MJ. Host factors in coronavirus replication. Current Topics in Microbiology and Immunology. Springer Verlag; 2018. pp. 1–42. doi:10.1007/82_2017_25

119. Ribeiro RM, Li H, Wang S, Stoddard MB, Learn GH, Korber BT, et al. Quantifying the diversification of hepatitis C virus (HCV) during primary infection: Estimates of the in vivo mutation rate. PLoS Pathog. 2012;8. doi:10.1371/journal.ppat.1002881

120. Li DK, Chung RT. Overview of direct-acting antiviral drugs and drug resistance of hepatitis C virus. Methods in Molecular Biology. Humana Press Inc.; 2019. pp. 3–32. doi:10.1007/978-1-4939-

8976-8_1

121. Perales C, Quer J, Gregori J, Esteban JI, Domingo E. Resistance of hepatitis C virus to inhibitors: Complexity and clinical implications. Viruses. MDPI AG; 2015. pp. 5746–5766. doi:10.3390/v7112902

122. McGivern DR, Masaki T, Williford S, Ingravallo P, Feng Z, Lahser F, et al. Kinetic analyses reveal potent and early blockade of hepatitis C virus assembly by NS5A inhibitors. Gastroenterology. 2014;147. doi:10.1053/J.GASTRO.2014.04.021

123. Bhattacharjee C, Singh M, Das D, Chaudhuri S, Mukhopadhyay A. Current therapeutics against HCV. VirusDisease. 2021;32: 228. doi:10.1007/S13337-021-00697-0

124. Alazard-Dany N, Denolly S, Boson B, Cosset FL. Overview of hcv life cycle with a special focus on current and possible future antiviral targets. Viruses. MDPI AG; 2019. p. 30. doi:10.3390/v11010030

125. Kaptein SJF, Goethals O, Kiemel D, Marchand A, Kesteleyn B, Bonfanti JF, et al. A pan-serotype dengue virus inhibitor targeting the NS3–NS4B interaction. Nat 2021 5987881. 2021;598: 504–509. doi:10.1038/s41586-021-03990-6

126. Nagy PD, Pogany J. The dependence of viral RNA replication on co-opted host factors. Nat Rev Microbiol. 2012;10: 137–149. doi:10.1038/nrmicro2692

127. Hafirassou ML, Meertens L, Umaña-Diaz C, Labeau A, Dejarnac O, Bonnet-Madin L, et al. A global interactome map of the dengue virus NS1 identifies virus restriction and dependency host factors. Cell Rep. 2017;21: 3900–3913. doi:10.1016/j.celrep.2017.11.094

128. Lee JS, Tabata K, Twu WI, Rahman MS, Kim HS, Yu JB, et al. RACK1 mediates rewiring of intracellular networks induced by hepatitis C virus infection. PLoS Pathog. 2019;15: e1008021. doi:10.1371/journal.ppat.1008021

129. Majzoub K, Hafirassou ML, Meignin C, Goto A, Marzi S, Fedorova A, et al. RACK1 controls IRES-mediated translation of viruses. Cell. 2014;159: 1086–1095. doi:10.1016/j.cell.2014.10.041

130. Adams DR, Ron D, Kiely PA. RACK1, A multifaceted scaffolding protein: Structure and function. Cell Commun Signal. 2011;9: 22. doi:10.1186/1478-811X-9-22

131. Kobayashi K, Koike S. Cellular receptors for enterovirus A71. J Biomed Sci 2020 271. 2020;27: 1–

12. doi:10.1186/S12929-020-0615-9

132. Qing J, Wang Y, Sun Y, Huang J, Yan W, Wang J, et al. Cyclophilin A associates with enterovirus-71 virus capsid and plays an essential role in viral infection as an uncoating regulator. PLoS Pathog. 2014;10: e1004422. doi:10.1371/journal.ppat.1004422

133. Dawar FU, Tu J, Khattak MNK, Mei J, Lin L. Cyclophilin a: A key factor in virus replication and potential target for anti-viral therapy. Curr Issues Mol Biol. 2017;21: 1–20. doi:10.21775/cimb.021.001

134. Bauer L, Lyoo H, van der Schaar HM, Strating JR, van Kuppeveld FJ. Direct-acting antivirals and host-targeting strategies to combat enterovirus infections. Current Opinion in Virology. Elsevier B.V.; 2017. pp. 1–8. doi:10.1016/j.coviro.2017.03.009

135. Paul D, Hoppe S, Saher G, Krijnse-Locker J, Bartenschlager R. Morphological and biochemical characterization of the membranous hepatitis C virus replication compartment. J Virol. 2013;87: 10612–27. doi:10.1128/JVI.01370-13

136. Tabata K, Prasad V, Paul D, Lee JY, Pham MT, Twu WI, et al. Convergent use of phosphatidic acid for hepatitis C virus and SARS-CoV-2 replication organelle formation. Nat Commun 2021 121. 2021;12: 1–15. doi:10.1038/s41467-021-27511-1

137. Ford Siltz LA, Viktorova EG, Zhang B, Kouiavskaia D, Dragunsky E, Chumakov K, et al. New small-molecule inhibitors effectively blocking picornavirus replication. J Virol. 2014;88: 11091–11107. doi:10.1128/jvi.01877-14

138. LaMarche MJ, Borawski J, Bose A, Capacci-Daniel C, Colvin R, Dennehy M, et al. Anti-hepatitis C virus activity and toxicity of type III phosphatidylinositol-4-kinase beta inhibitors. Antimicrob Agents Chemother. 2012;56: 5149–5156. doi:10.1128/AAC.00946-12

139. Melia CE, van der Schaar HM, Lyoo H, Limpens RWAL, Feng Q, Wahedi M, et al. Escaping host factor PI4KB inhibition: Enterovirus genomic RNA replication in the absence of replication organelles. Cell Rep. 2017;21: 587–599. doi:10.1016/j.celrep.2017.09.068

140. V'kovski P, Kratzel A, Steiner S, Stalder H, Thiel V. Coronavirus biology and replication: implications for SARS-CoV-2. Nature Reviews Microbiology. Nature Publishing Group; 2021. pp. 155–170. doi:10.1038/s41579-020-00468-6

S1 Supporting material: Model selection process.

S1 Supporting data

Drug A	Drug B	HCV	DENV	CVB3
TC formation (k_1)	-	0.96	1	1
Translation (k_2)	-	0.99	0.99	1
Polyprotein cleavage (k_c)	-	0.995	1	1
RC formation (k_{Pin})	-	0.99	1	-
RNA synthesis (k_{4p} and k_{4m})	-	0.89	0.865	0.995
Viral export (k_{Pout})	-	1	1	1
Virus assembly and release (k_p)	-	1	1	1
TC formation (k_1)	***RNA synthesis (k_{4p} and k_{4m})***	**0.76**	**0.85**	0.993
TC formation (k_1)	***RC formation (k_{Pin})***	0.85	0.99	1
Translation (k_2)	***RNA synthesis (k_{4p} and k_{4m})***	0.90	**0.85**	0.99
Translation (k_2)	***RC formation (k_{Pin})***	0.96	0.98	0.991
Polyprotein cleavage (k_c)	***RNA synthesis (k_{4p} and k_{4m})***	0.90	0.87	**0.98**
Polyprotein cleavage (k_c)	***RC formation (k_{Pin})***	0.997	0.999	1

S1 Table: Critical drug efficacy constants in mono and combination therapy and an in-silico drug administration in steady state (100 h pi). For simplicity, we assume that in combination therapy, both drugs have the same efficacy. The lowest critical drug efficacies to clear the virus-specific infection is highlighted in red (TC = translation complex, RC = replicase complex)

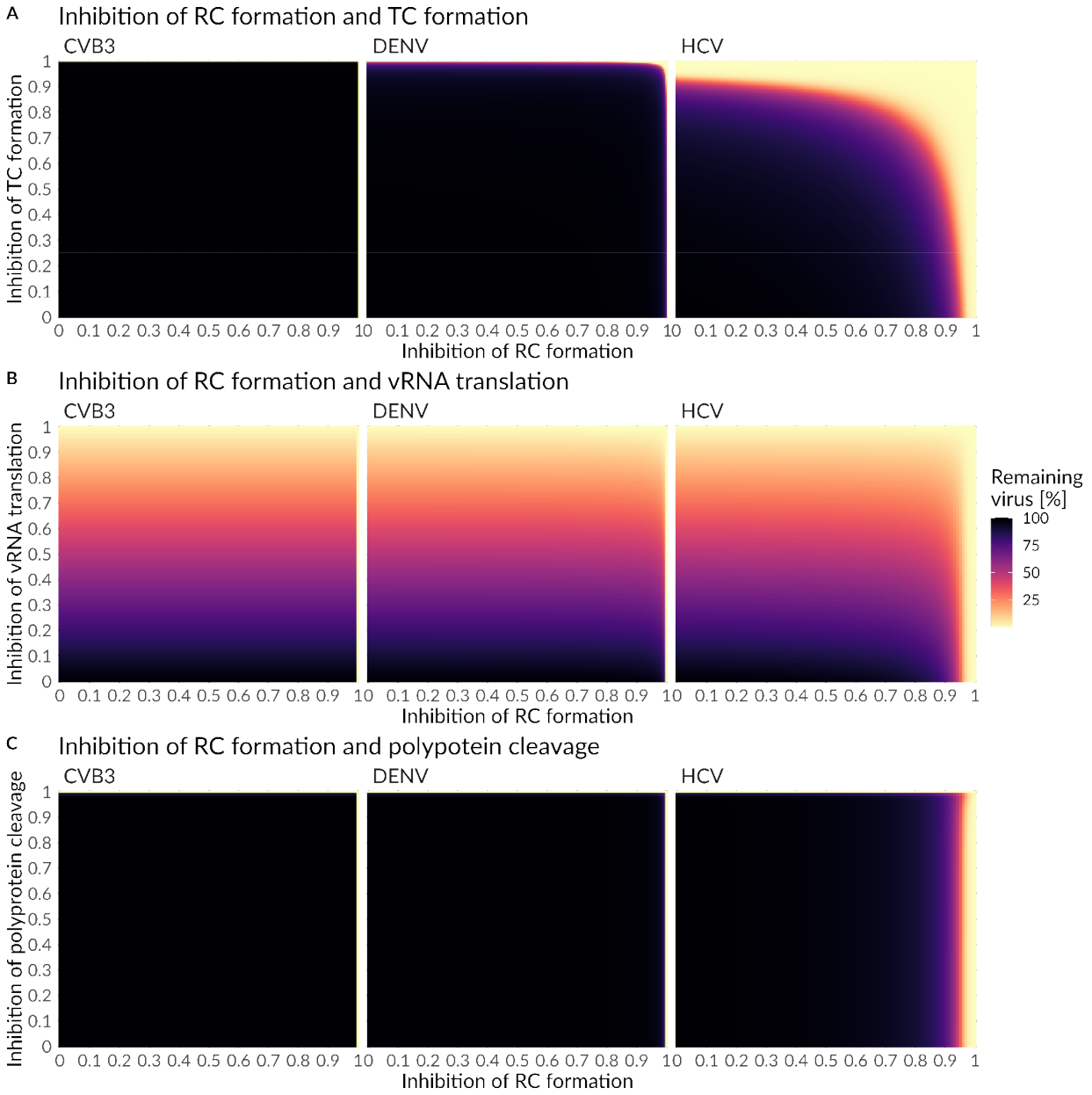

*S1 Figure: Combined drug effect on **A)** replicase complex (RC) formation and formation of translation complex (TC) **B)** replicase complex (RC) formation and polyprotein cleavage and **C)** replicase complex (RC) formation and vRNA translation and drug administration in steady state (100 h pi). A successful drug treatment leads to a more than 99% viral eradication (light yellow), while an ineffective drug treatment leads to 100% remaining virus (black).*

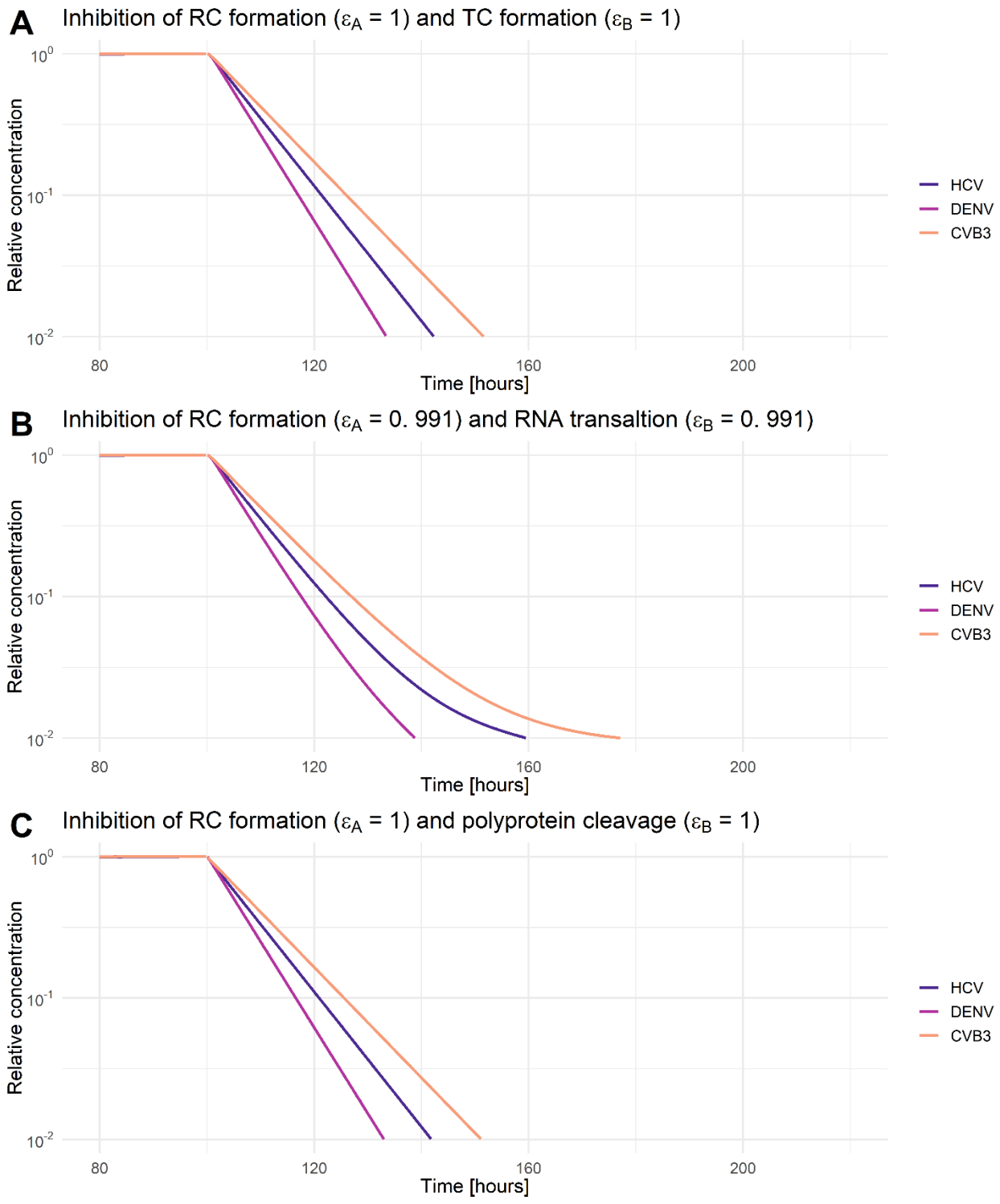

*S2 Figure: Relative virus decay under combination therapy that clears HCV, DENV, and CVB3 infections. A combined drug effect on **A)** formation of replicase complex (RC) and formation of translation complex (TC), **B)** formation of replicase complex (RC) and translation, and **C)** formation of replicase complex (RC) and polyprotein cleavage. Initiation of treatment was in steady state (100 h pi). The drug efficacy*

constant (ε_A and ε_B) were chosen as minimal efficacies to clear all three viruses. For comparability, virus-specific concentrations in steady state have been normalized to their virus-specific pre-treatment steady state concentration. A successful drug treatment leads to a more than 99% viral eradication (light yellow), while an ineffective drug treatment leads to 100% remaining virus (black) (see S1 Supporting data).